SUPPORTING INFORMATION

Increase in pore size and gas uptake capacity in indium-organic framework material.

Jinjie Qian,[a,b] Feilong Jiang,[a] Daqiang Yuan,[a] Xingjun Li,[a,b] Linjie Zhang,[a,b] Kongzhao Su,[a,b] and Maochun Hong*[a]

[†]Key Laboratory of Optoelectronic Materials Chemistry and Physics, State Key Laboratory of Structure Chemistry, Fujian Institute of Research on the Structure of Matter, Chinese Academy of Sciences, Fuzhou, Fujian, 350002, China

[§]Graduate School of the Chinese Academy of Sciences, Beijing, 100049, China

*To whom correspondence should be addressed: E-mail:hmc@fjirsm.ac.cn; Fax: +86-591-83794946; Tel: +86-591-83792460

Table of Contents

S1. General Experimental Procedures

1.1. Research background of InOF-2

When repeating the preparation of the solvated framework complex [Me$_2$NH$_2$][In(BPTC)] (labelled as **InOF-0** here) under the solvothermal conditions reported by Martin Schröder group,[S1] interestingly, we increased the molar ratio of metal salts In(NO$_3$)$_3$ and BPTC ligands to 4:1, thus to get a highly water-stable indium-organic framework [In$_2$(OH)$_2$(BPTC)]·6H$_2$O (**InOF-1**), which is recently published in Chem. Commun..[S2] Under the exactly same conditions described in the former paper, however, sometimes very few of new crystals, an isomeric structure of the compound **InOF-0** with totally different shape confirmed by single crystal X-ray diffraction analysis (Figure. S1), were obtained. Therefore a lot of effort has been directed towards looking for the most optimized conditions of preparing this new crystal, and this process is concluded in Table S1.

Figure S1. Photograph of **InOF-2** under lab microscope.

1.2. Search for the Most Optimized Conditions for InOF-2.

Table S1. A series of conditions were tested, including metal salt, Metal:Ligand (M:L) molar ratio, concentration, reaction time etc., to look for the most optimized conditions for InOF-2.

● Optimised conditions for InOF-2

Salt	Batch	M:L ratio	Solvents	Concentration	Results	Notes
$InCl_3$	1	2.0:1.0	DMF/CH_3CN	5 ml/5 ml	◆ , Pure & good quality, InOF-0	*Temp(^oC)=85; *Reation time=7 days; *All reactions with an additional 0.2 ml HNO_3 (65 wt *Obtained crystals in good quality was in **BOLD** type.
	2	1.0:1.0	DMF/CH_3CN	5 ml/5 ml	◆ , Pure & good quality, InOF-0	
	3	1.0:2.0	DMF/CH_3CN	5 ml/5 ml	Precipitate	
	4	1.0:1.0	DMF/CH_3CN	2.5 ml/7.5 ml	Precipitate	
	5	1.0:1.0	DMF/CH_3CN	7.5 ml/2.5 ml	◆ , Tiny & good quality, InOF-0	
	6	1.0:1.0	DMF	10 ml	Tiny & poor quality, InOF-0	
	7	1.0:1.0	CH_3CN	10 ml	Precipitate	
	8	1.0:1.0	DMF/CH_3OH	5 ml/5 ml	Precipitate	
	9	1.0:1.0	DMF/CH_3CH_2OH	5 ml/5 ml	Precipitate	
	10	1.0:1.0	DMF/1,4-dioxane	5 ml/5 ml	◆ , Pure & good quality, InOF-0	
	11	1.0:1.0	DMF/THF	5 ml/5 ml	◆ , Pure & good quality, InOF-0	
	12	1.0:1.0	DMA/CH_3CN	5 ml/5 ml	Clear	
	★13	1.0:1.0	DEF/CH_3CN	5 ml/5 ml	▮ , Pure & good quality, InOF-2	
	14	1.0:1.0	DMA	10 ml	Tiny & poor quality, InOF-0	
	15	1.0:1.0	DEF	10 ml	Tiny & poor quality, InOF-2	

Salt	Batch	M:L ratio	Solvents	Concentration	Results	Notes
$In(NO_3)_3$	16	1.0:1.0	DMF/CH_3CN	5 ml/5 ml	◆ , Pure & good quality, InOF-0	*Temp(^oC)=85; *Reation time=7 days; *All reactions with an additional 0.2 ml HNO_3 (65 wt *Obtained crystals in good quality was in **BOLD** type.
	17	1.0:1.0	DMF/CH_3CN	4 ml/4 ml	◆ , Pure & good quality, InOF-0	
	18	1.0:1.0	DMF/CH_3CN	3 ml/3 ml	◆ , Pure & good quality, InOF-0	
	19	1.0:1.0	DMF/CH_3CN	2.5 ml/7.5 ml	Precipitate	
	20	1.0:1.0	DMF/CH_3CN	7.5 ml/2.5 ml	Tiny & poor quality, InOF-0	
	21	1.0:1.0	DMF	10 ml	Tiny & poor quality, InOF-0	
	22	1.0:1.0	CH_3CN	10 ml	Precipitate	
	23	1.0:1.0	DMF/CH_3OH	5 ml/5 ml	Precipitate	
	24	1.0:1.0	DMF/CH_3CH_2OH	5 ml/5 ml	Precipitate	
	25	1.0:1.0	DMF/1,4-dioxane	5 ml/5 ml	◆ , Pure & good quality, InOF-0	
	26	1.0:1.0	DMF/THF	5 ml/5 ml	Tiny & Poor quality, InOF-0	
	27	1.0:1.0	DMA/CH_3CN	5 ml/5 ml	Tiny & poor quality, InOF-0	
	28	1.0:1.0	DEF/CH_3CN	5 ml/5 ml	Tiny & poor quality, InOF-2	
	29	1.0:1.0	DMA	10 ml	Tiny & Poor quality, InOF-0	
	30	1.0:1.0	DEF	10 ml	Tiny & poor quality, InOF-2	
	31	4.0:1.0	DMF/CH_3CN	5 ml/5 ml	▮ , Pure & good quality, InOF-1	

★ The most optimised conditions of InOF-2 as reported in the manuscript.

InOF-0=$Me_2NH_2[In(BPTC)].(DMF).(CH_3CN).(H_2O)_4$ Reported by Martin Schröder (DOI: 10.1039/b814155j).

InOF-1=$[In_2(OH)_2(BPTC)].6H_2O$ Reported by our group (DOI: 10.1039/c2cc35068h).

InOF-2= $Et_2NH_2[In(BPTC)]\cdot5H_2O$ Reported in this work. **(CCDC No.= 928842)**

1.3. Materials and Methods.

All the reactions were carried in 23 ml glass vials under autogenous pressure. All the reactants are of reagent-grade quality and used as purchased commercially without further purification. The power X-ray diffraction patterns (PXRD) and Variable-temperature X-ray Diffraction (VT-XRD) were collected by a Rigaku D/MAX2500 X-ray diffractometer using Cu Kα radiation (λ=0.154 nm). Thermogravimetric analyses (TGA) were recorded on a NETZSCH STA 449C unit at a heating rate of 10 ^{o}C· min^{-1} under flowing nitrogen atmosphere. Thermogravimetric analysis-mass spectrometry (TGA-MS) experiments had been performed on a NETZSCH STA 449C-QMS 403 C. Single gas adsorption measurements were performed in the ASAP (Accelerated Surface Area and Porosimetry) 2020 System. Elemental analyses for C, H, N were carried out on a German Elementary Vario EL III instrument. Inductively coupled plasma OES spectrometer (ICP) was tested on a Jobin Yvon Ultima2.
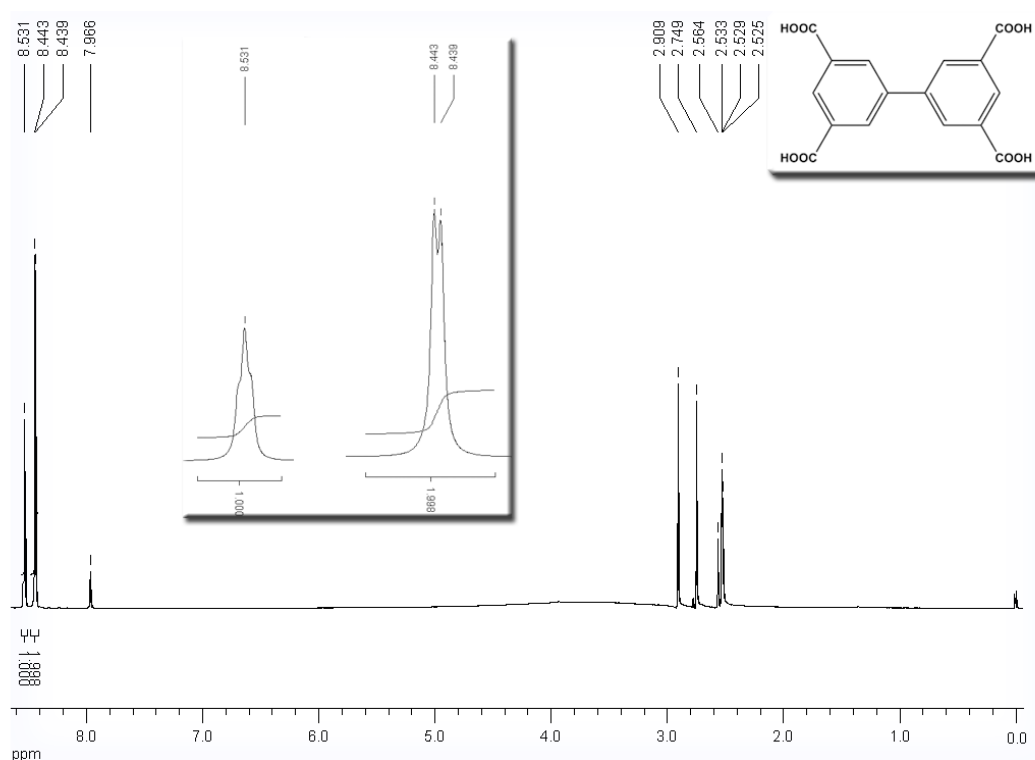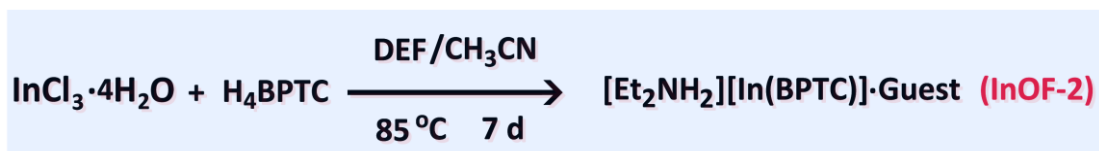

Figure S2. ^{1}H-NMR spectrum of the H$_4$BPTC ligand was measured in DMSO-d$_6$.

S4

1.4. Synthesis of [Et₂NH₂][In(BPTC)]·5H₂O (InOF-2).

A mixture of $InCl_3 \cdot 4H_2O$ (0.10 mmol, 22 mg) and H_4BPTC (0.10 mmol, 33 mg, H_4BPTC = Biphenyl-3,3',5,5'-tetracarboxylic acid) in N,N'-diethylformamide (DEF) (5 ml) and CH_3CN (5 ml) with an additional HNO_3 (0.2 ml, 65 wt %) was sealed in a 23 ml glass vial, which was heated at 85 ^{o}C for 7 days, and cooled down to room-temperature. After washed by fresh C_2H_5OH, the light yellow bulk crystals (**InOF-2, M=605**) were obtained in *ca.* 50% yield based on the BPTC ligand. Elemental analysis was calculated for **InOF-2**: C, 39.69%; H, 4.66%; N2.31%. Found: C, 39.98%; H, 4.52%; N, 1.99%. The phase purity of the sample was confirmed by powder X-ray diffraction (PXRD) and more details are shown below in Section S4.

$$InCl_3 \cdot 4H_2O + H_4BPTC \xrightarrow[85\,^\circ C \quad 7\,d]{DEF/CH_3CN} [Et_2NH_2][In(BPTC)] \cdot Guest \quad (InOF\text{-}2)$$

Scheme S1. The synthesis of **InOF-2**.

S2. Single-Crystal X-ray Crystallography

The structures data of compound **InOF-2** was collected on a Rigaku Mercury CCD diffractometer equipped with a graphite-monochromated Mo Kα radiation (λ=0.71073Å) at room temperature and the structure was resolved by the direct method and refined by full-matrix least-squares fitting on F^2 by SHELX-97. [S3] The hydrogen atoms of the water molecules were found in the electron density map and refined by riding. Crystallographic data and structure refinement parameters at 298 and 333 K for **InOF-2** are listed in Table S2. We employed PLATON/SQUEEZE[S4] to calculate the contribution to the diffraction from the solvent region and thereby produced a set of solvent-free diffraction intensities. The final formula was calculated from the SQUEEZE[S4] results combined with elemental analysis data and TGA data. More details on the crystallographic studies as well as atomic displacement parameters are given in Supporting Information as CIF files. Crystallographic data for the structures reported in this paper have been deposited The following crystal structure has been deposited at the Cambridge Crystallographic Data Centre and allocated the deposition number (CCDC No.) 928842 for **InOF-2**.

Table S2. Crystal Data and Structure Refinement for InOF-2 at 298 K and 333 K.

Items	InOF-2-T298K	InOF-2-T333K	InOF-2-Li$^+$-T298K
chemical formula	$C_8H_3In_{0.50}O_4$	$C_8H_3In_{0.50}O_4$	$C_8H_3In_{0.50}O_4$
formula mass	220.51	220.51	220.51
crystal system	Tetragonal	Tetragonal	Tetragonal
space group	$I4_32_12$ (#. 96)	$I4_12_12$ (#. 92)	$I4_12_12$ (#. 92)
a (Å)	17.8210(5)	17.9238(3)	17.7549(1)
b (Å)	17.8210(5)	17.9238(3)	17.7549(1)
c (Å)	11.2345(6)	11.0545(3)	11.2325(1)
α (°)	90.00	90.00	90.00
β (°)	90.00	90.00	90.00
γ (°)	90.00	90.00	90.00
unit cell volume	3567.9(2)	3551.5 (1)	3540.82(4)
temperature (K)	298(2)	333(2)	298(2)
Z	8	8	8
F(000)	860	860	860
no. of reflections measured	22976	10824	10646
no. of independent reflections	3116	3126	3351
R_{int}	0.0335	0.0500	0.0371
final R1 values (I>2σ(I))	0.0228	0.0389	0.0365
final wR (F^2) values (I>2σ(I))	0.0663	0.0869	0.1322
goodness of fit on F^2	1.133	0.975	1.028
flack parameter	0.00(2)	0.00(2)	0.00(2)

S3. Additional X-ray Crystal Structural and Topological Figures
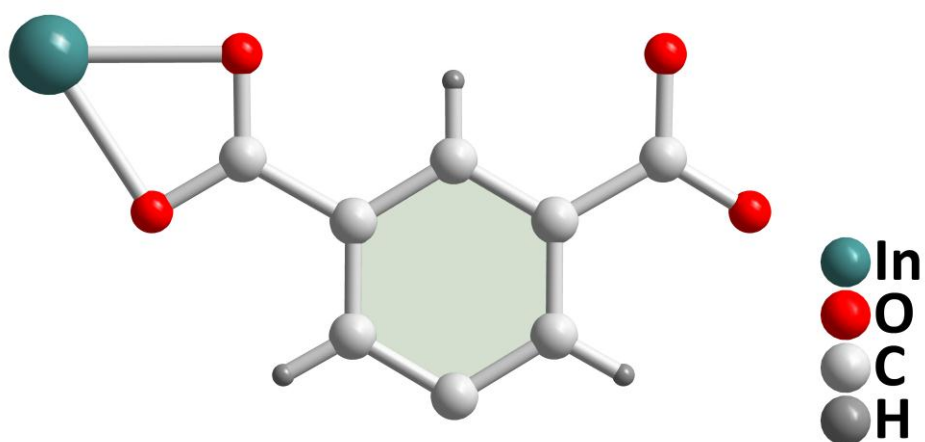
Figure S3. The asymmetric unit of **InOF-2**.
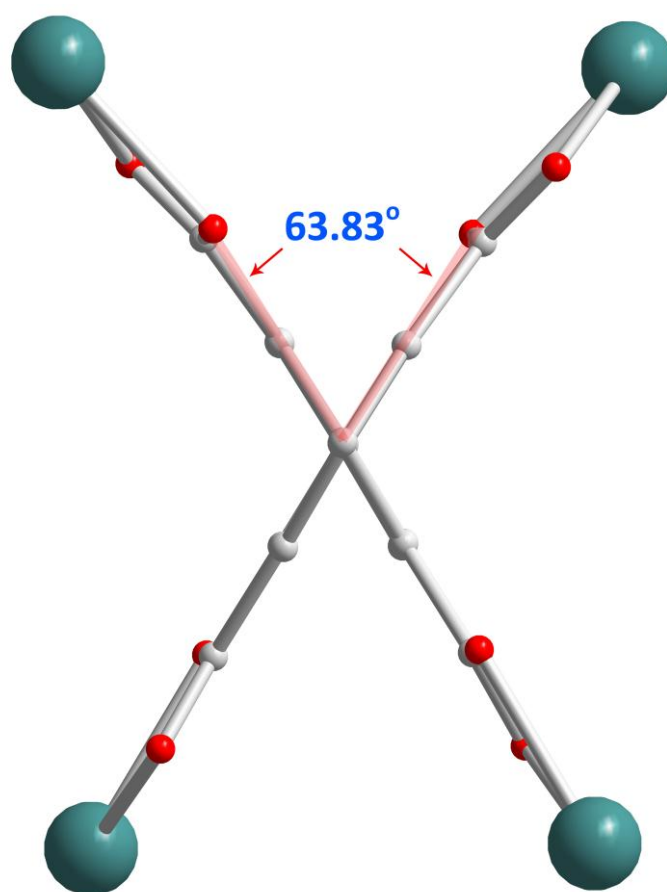
Figure S4. The dihedral angel of BPTC ligand with a value of 63.83° observed in **InOF-2** at 298 K.
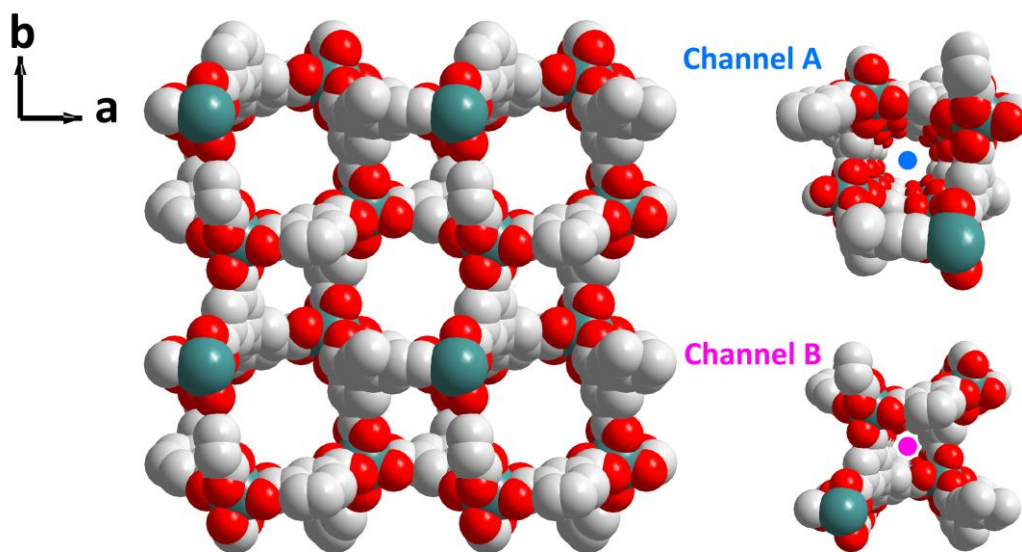
Figure S5. A space-filling view of **InOF-2** along the *c* axis, which consists of two kinds of channels, that is, Channel-A and Channel-B.
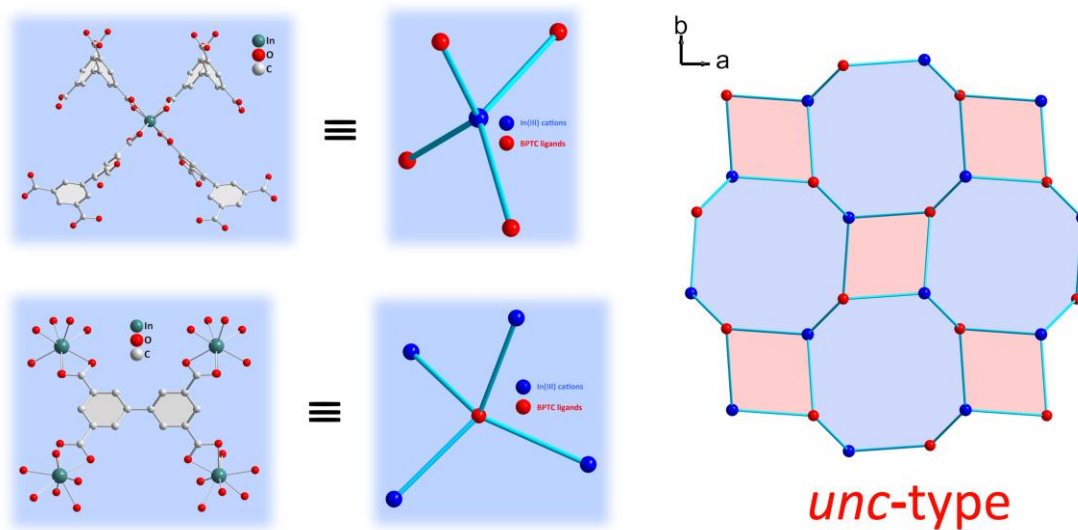

Figure S6. Topological analysis shows that this compound is uninodal *unc*-type three-dimensional network where 4-connected In(III) nodes and 4-connected BPTC nodes are topologically equal.

S4. Powder X-Ray Diffraction
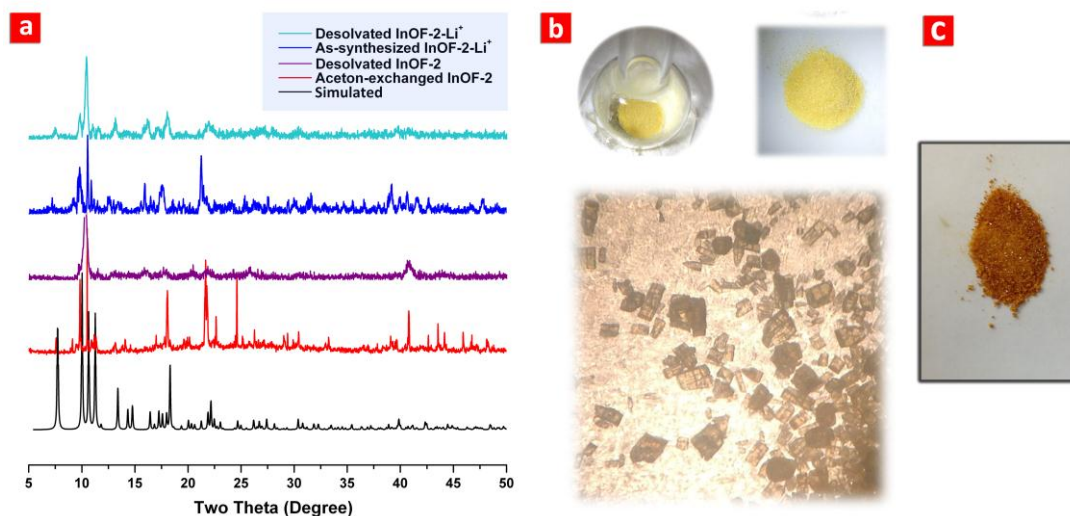
Figure S7. a) PXRD patterns for simulated **InOF-2**, acetone-exchanged **InOF-2**, desolvated **InOF-2**, as-synthesized Li$^+$-exchanged **InOF-2-Li$^+$**, and desolvated **InOF-2-Li$^+$**. b) Photograph of activated **InOF-2** materials at 373 K, under lab microscope. c) Photograph of activated **InOF-2** materials at 473 K.
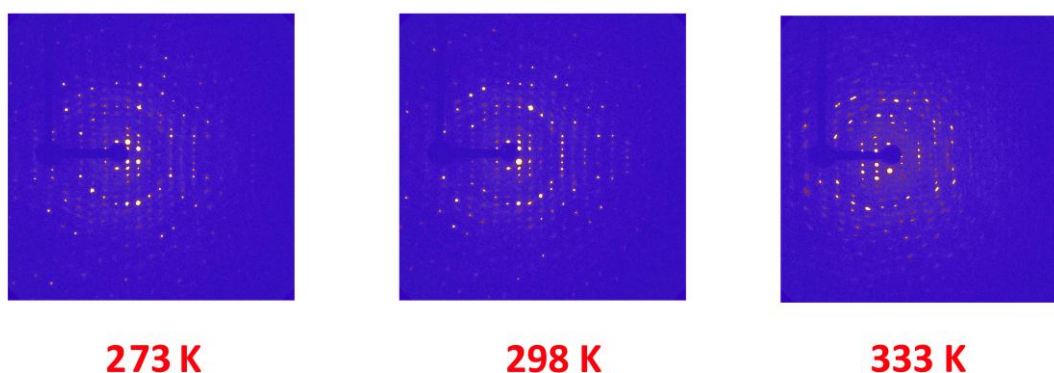
Figure S8. Bragg diffraction peaks of **InOF-2** at 273(2), 298(2), and 333(2) K.

S5. Thermal Gravimetric Plots
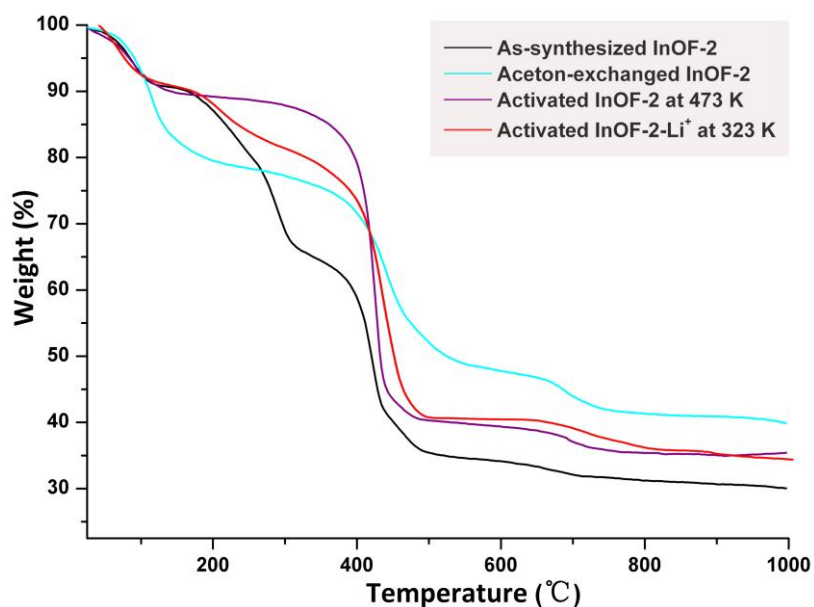
Figure S9. Thermal gravimetric analysis (TGA) for **InOF-2** with different treatment.

S6. Elemental Analysis

Table S3. Elemental analysis of InOF-2 with different treatment.

	C(%)	H(%)	N(%)	Li$^+$(%)
Calculated	39.69	4.66	2.31	0
As-synthesized	39.98	4.52	1.99	0
Acetone-exchanged	40.65	4.39	1.87	0
Li$^+$-exchanged	34.71	3.88	0	1.12

S7 Gas Sorption Test
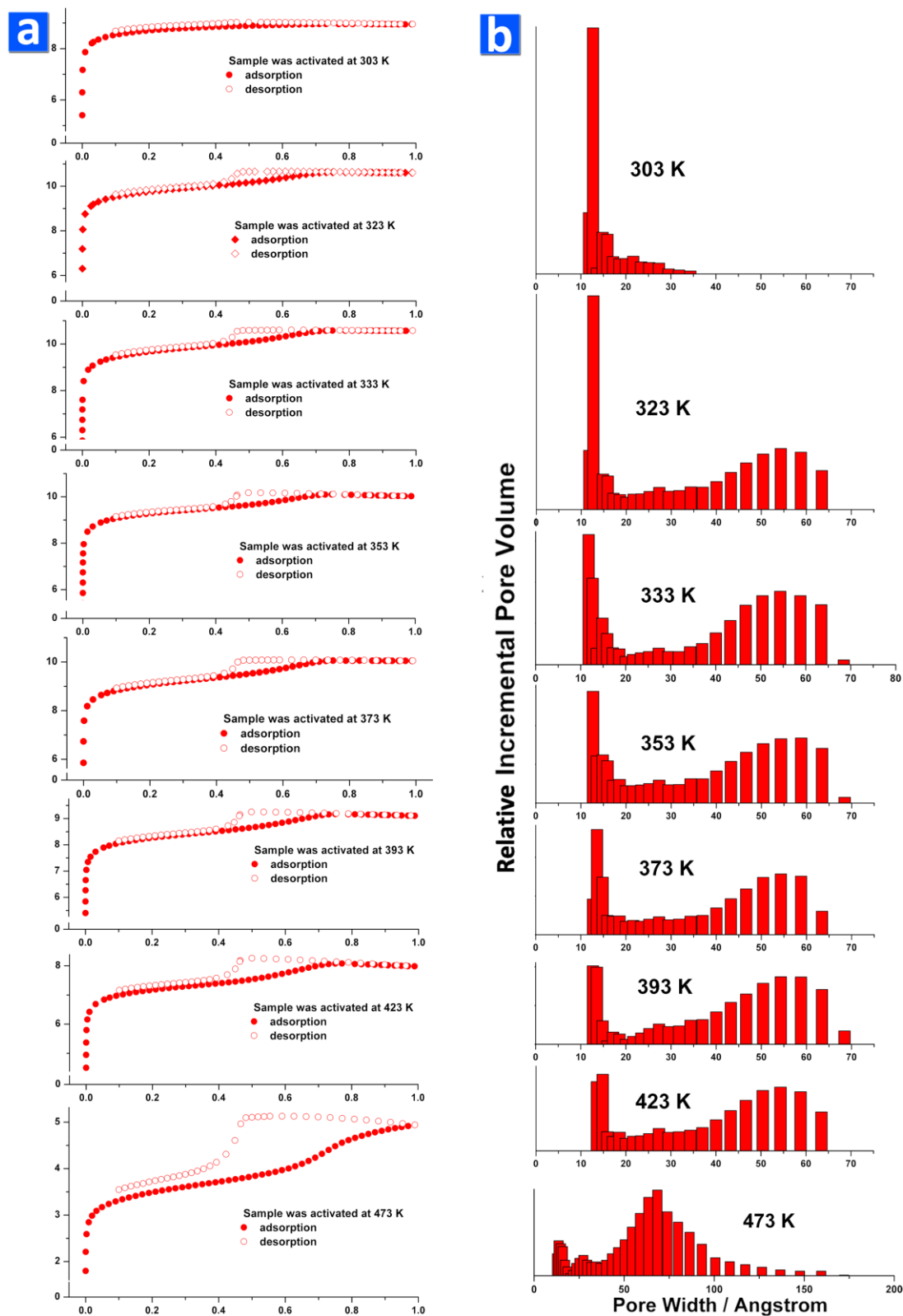
Figure S10. N_2 sorption isotherms at 77 K and pore size distribution of **InOF-2** sample at different activation temperature.
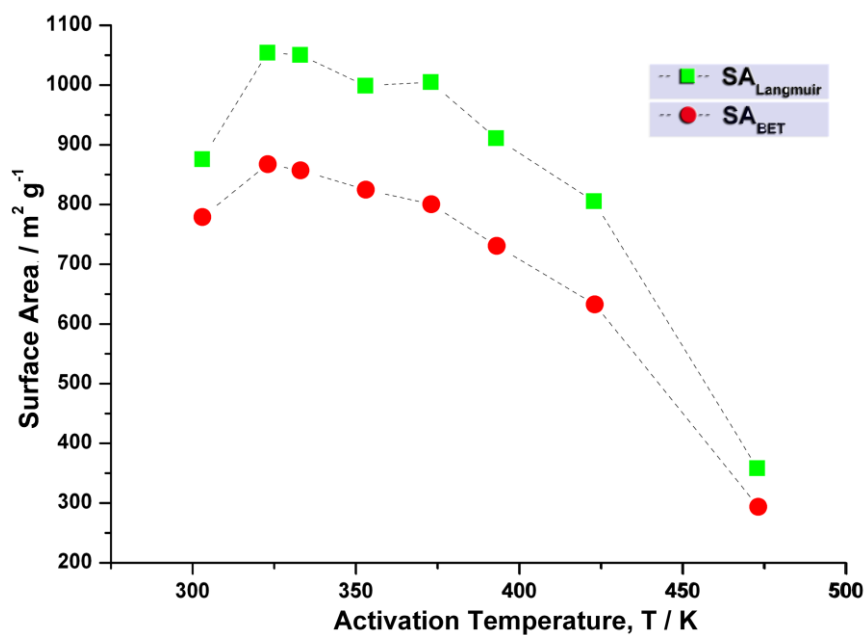
Figure S11. Brunauer-Emmett-Teller (BET) and Langmuir surface area of **InOF-2** sample at different activation temperature.
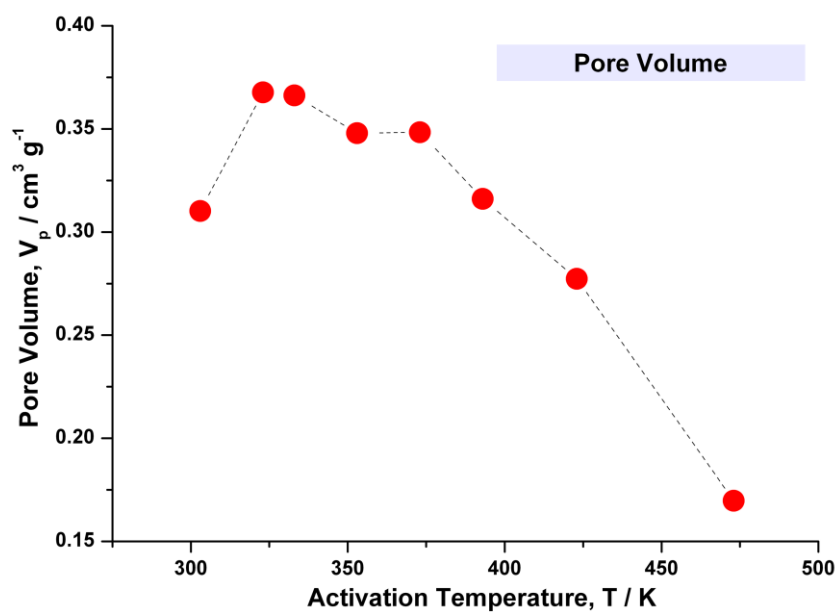
Figure S12. Pore volume of **InOF-2** sample at different activation temperature.

S13
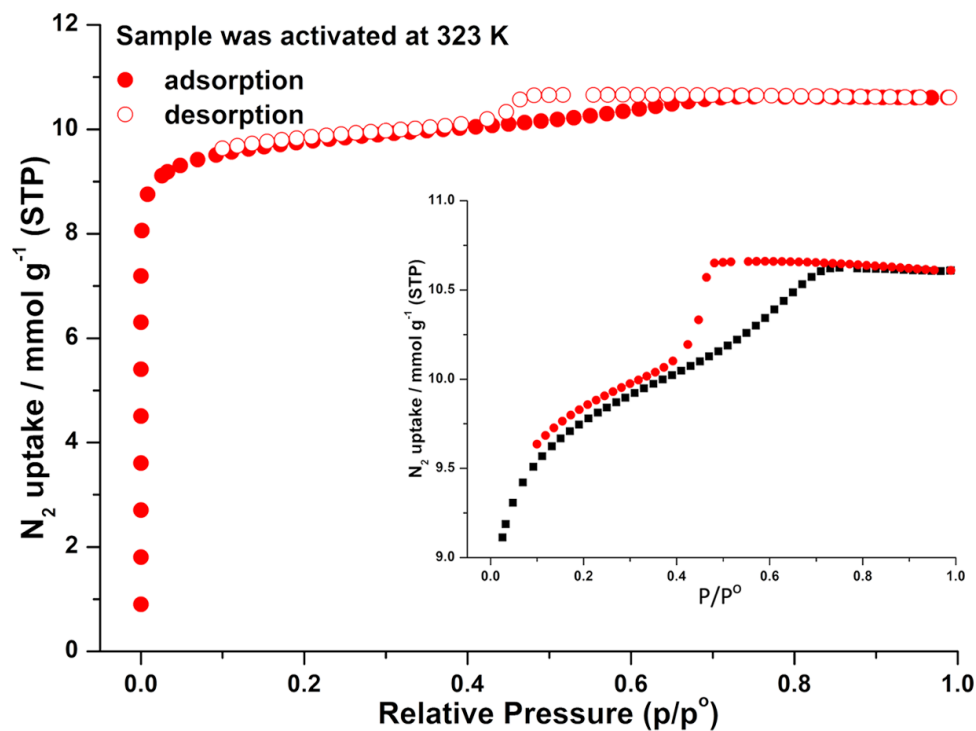
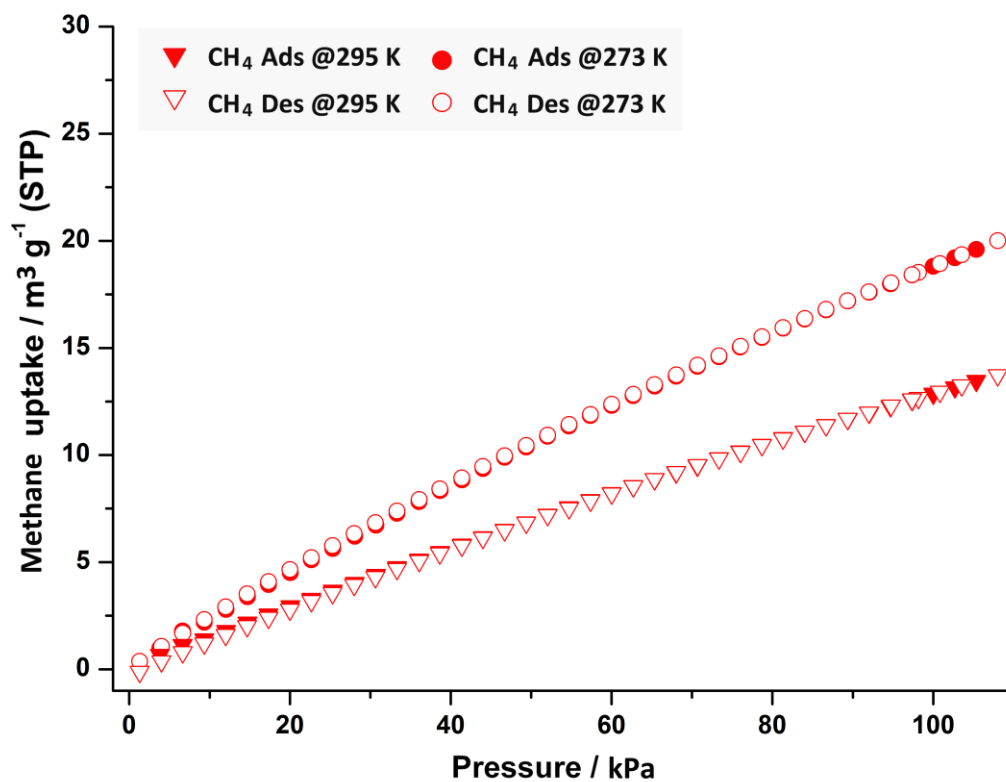**Figure S13**. N_2 sorption isotherms of **InOF-2** sample at 77 K activated under 323 K.

Figure S14. CH_4 sorption isotherms of **InOF-2** sample at 273/295 K activated under
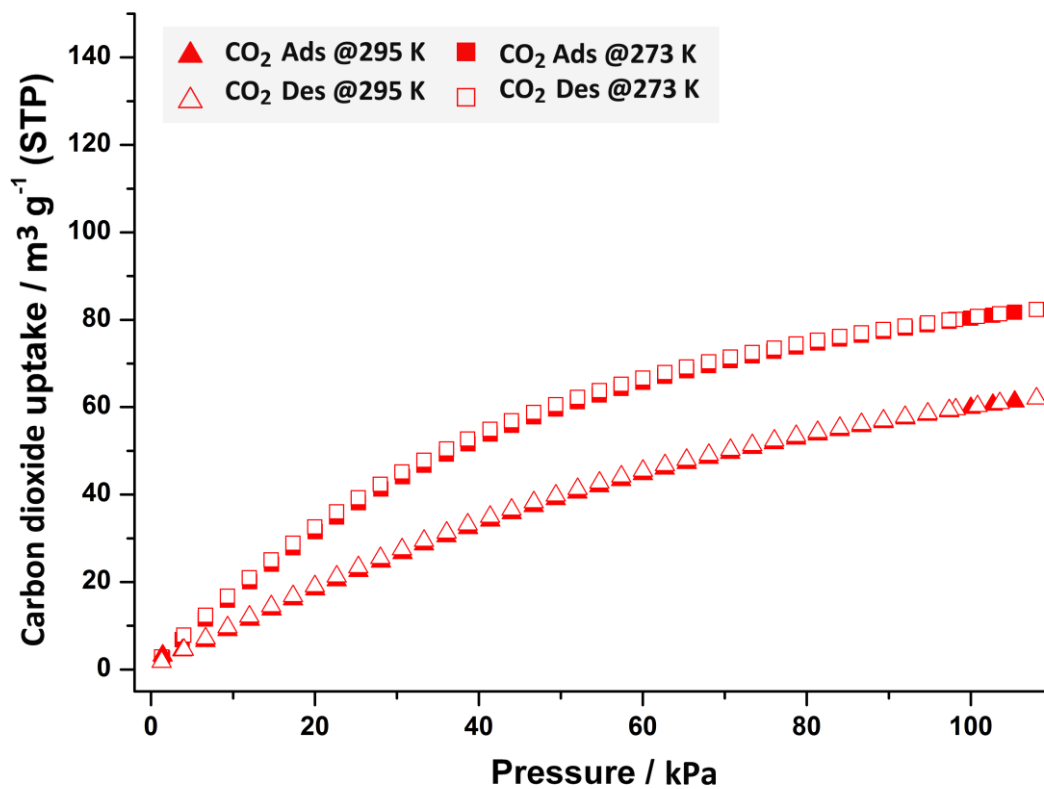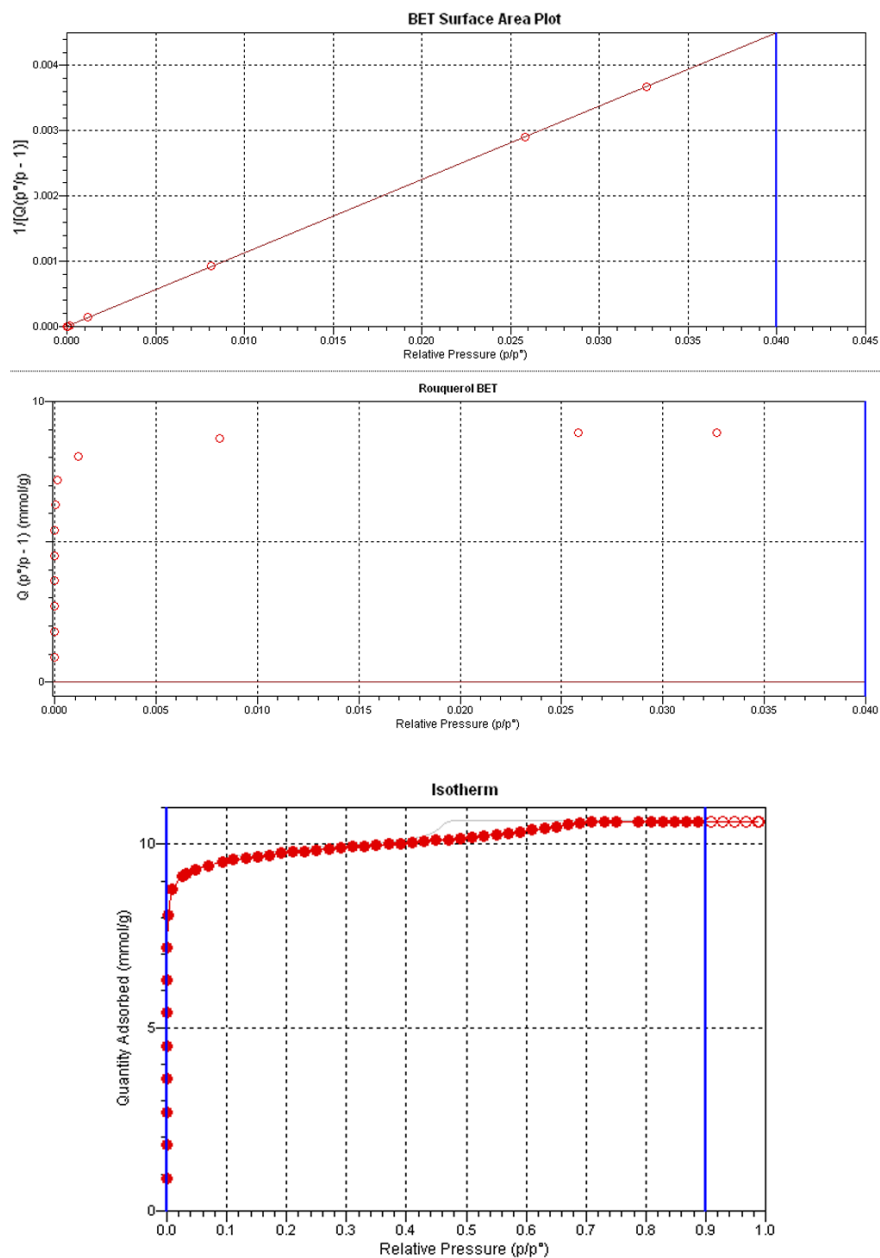
323 K.

Figure S15. CO_2 sorption isotherms of **InOF-2** sample at 273/295 K activated under 323 K.
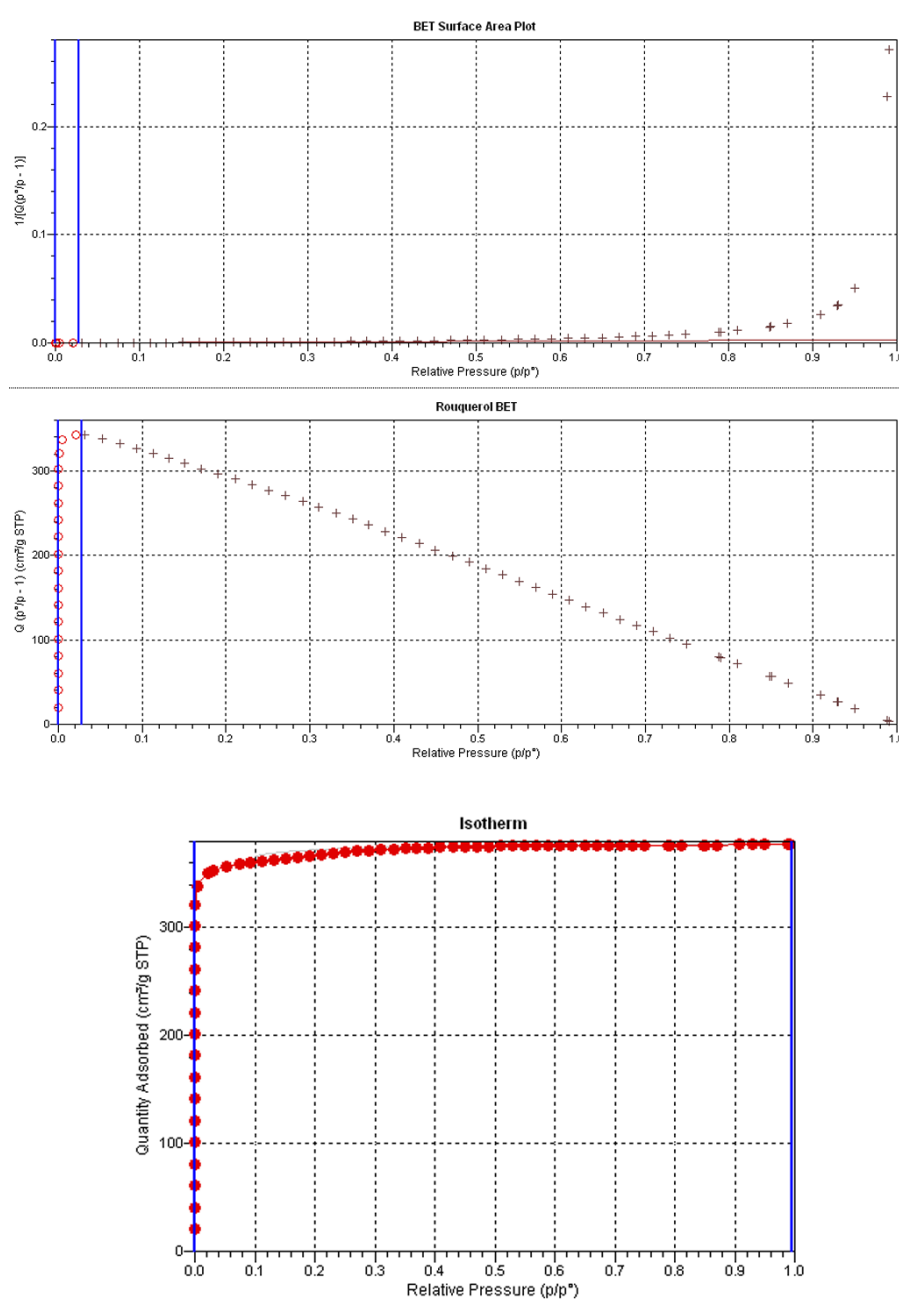
BET Surface Area Plot

Rouquerol BET

Isotherm

Summary

BET Surface Area: 867.2084 ± 1.4137 m²/g
Slope: 0.112510 ± 0.000183 g/mmol
Y-Intercept: 0.000004 ± 0.000002 g/mmol
C: 26698.396892
Qm: 8.88779 mmol/g
Correlation Coefficient: 0.9999867
Molecular Cross-Sectional Area: 0.1620 nm²

InOF-2

Figure S16: The BET surface area report of **InOF-2** sample obtained by N_2 adsorption data at 77 K on MicroActive Version 1.01.

S16

BET Surface Area Plot

Rouquerol BET

Isotherm

Summary
BET Surface Area: 1494.7277 ± 1.3297 m²/g
Slope: 0.002912 ± 0.000003 g/cm³ STP
Y-Intercept: 0.000000 ± 0.000000 g/cm³ STP
C: 29811.296660
Qm: 343.3631 cm³/g STP
Correlation Coefficient: 0.9999937
Molecular Cross-Sectional Area: 0.1620 nm²

InOF-2-Li$^+$

Figure S17: The BET surface area report of **InOF-2-Li$^+$** sample obtained by N_2

adsorption data at 77 K on MicroActive Version 1.01.

S17

S8. Heat of Adsorption (kJ mol^{-1})

CO_2 and CH_4 isotherms measured at 273 K and 296 K for **InOF-1**

were fit to the following Equation 1.[S5]

The adsorption isostere is represented by

$$\ln (P/P_0) = q_i/RT + C \qquad (1)$$

where

q_i = isosteric heat of adsorption

C = unknown constant

The isosteric heat of adsorption, q_i is determined by finding the slope

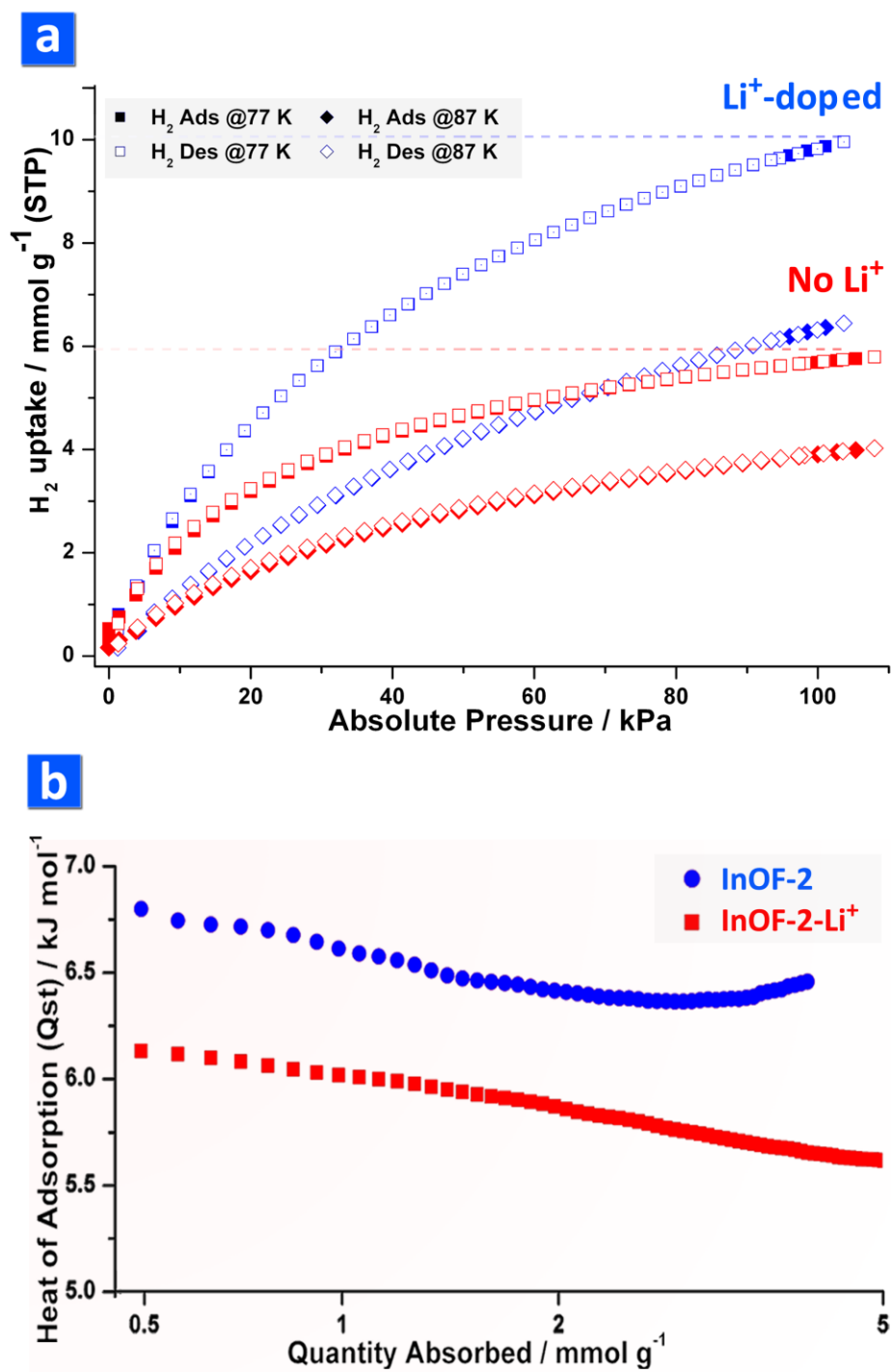of $\ln (P/P_0)$ as a function of $1/RT$ for a set of isotherms measured at

different temperatures.

Figure S18. a) CO_2 adsorption isotherms for **InOF-2-Li$^+$ (blue)** and **InOF-2 (red)** at 77 K and 87 K. b) the heat of adsorption (Q_{st})
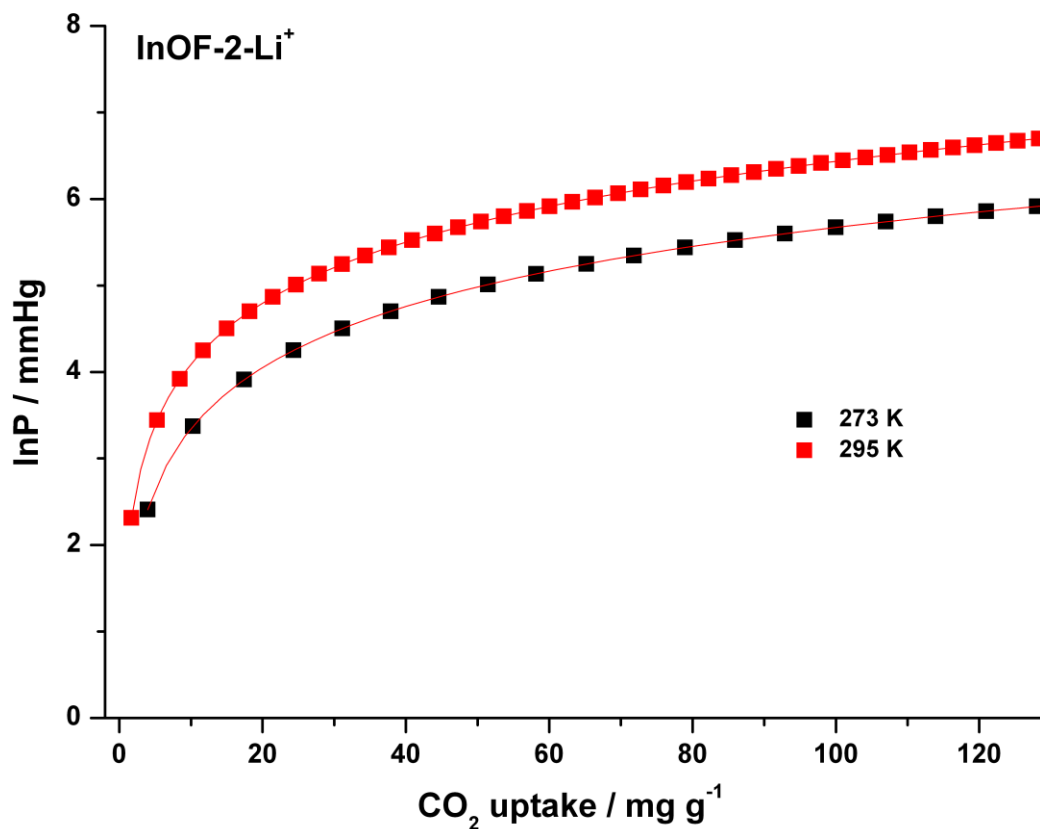
S19

Calculation of heats of adsorption for CO_2
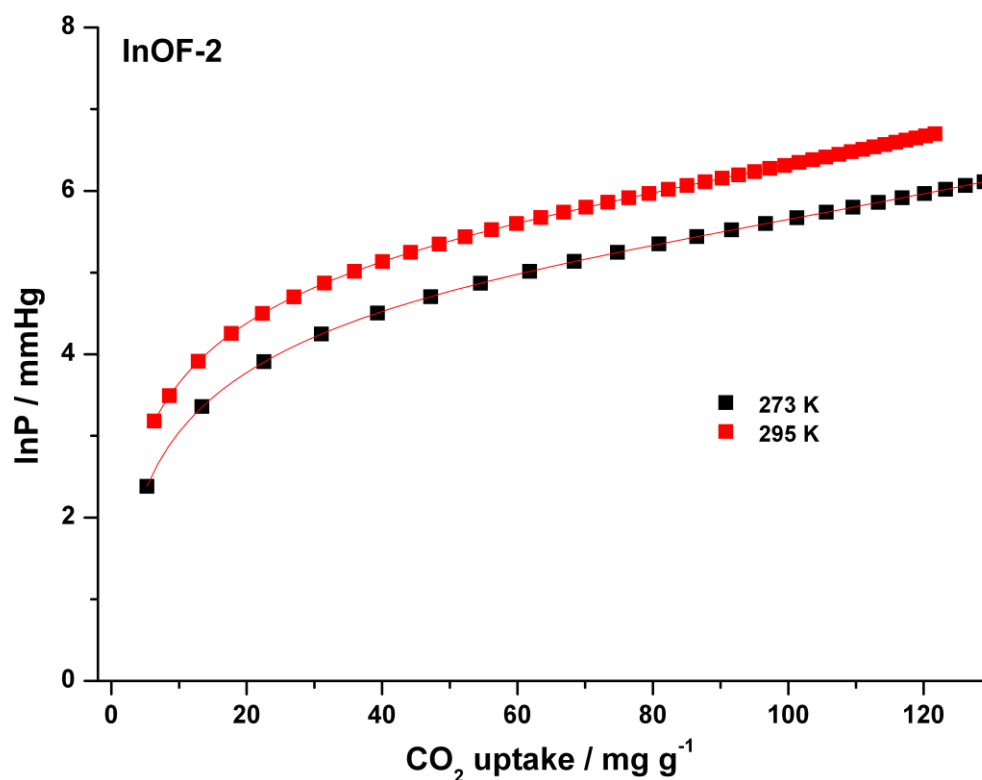
Figure S19. Nonlinear curve fitting of CO_2 adsorption isotherms for **InOF-2** at 273 K and 295 K.

y=ln(x)+1/k*(a0+a1*x+a2*x^2+a3*x^3+a4*x^4+a5*x^5)+(b0+b1*x+b2*x^2)

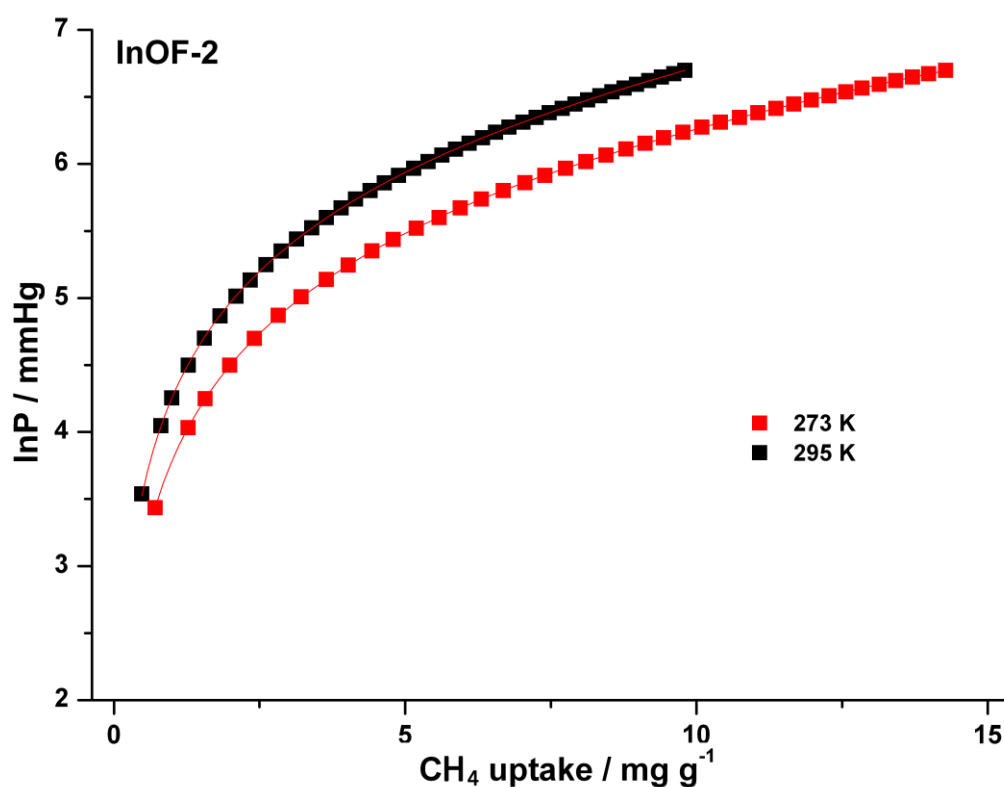|			Value	Standard Error
		a0*	-2221.42826	4.61757
		a1*	1.83873	0.14911
		a2*	-0.06162	0.00167
		a3*	3.11424E-4	2.39228E-5
		a4*	-1.35467E-6	1.56065E-7
ln(P)		a5*	2.73145E-9	3.69064E-10
		b0*	8.83193	0.01628
		b1*	-8.43667E-4	5.33023E-4
		b2*	1.27395E-4	3.78012E-6
		k	273	0
		k	295	0

Figure S20. Nonlinear curve fitting of CO_2 adsorption isotherms for **InOF-2-Li$^+$** at 273 K and 295 K.

y=ln(x)+1/k*(a0+a1*x+a2*x^2+a3*x^3+a4*x^4+a5*x^5)+(b0+b1*x+b2*x^2)

		Value	Standard Error
ln(P)	a0*	-2736.1694	1.52512
	a1*	1.02104	0.05146
	a2*	-0.01924	4.19228E-4
	a3*	4.13623E-5	1.76414E-6
	a4*	-1.11969E-7	7.56561E-9
	a5*	1.35806E-10	1.16922E-11
	b0*	11.05166	0.00529
	b1*	-0.00195	1.74105E-4
	b2*	4.47838E-5	1.21454E-6
	k	273	0
	k	295	0

S21
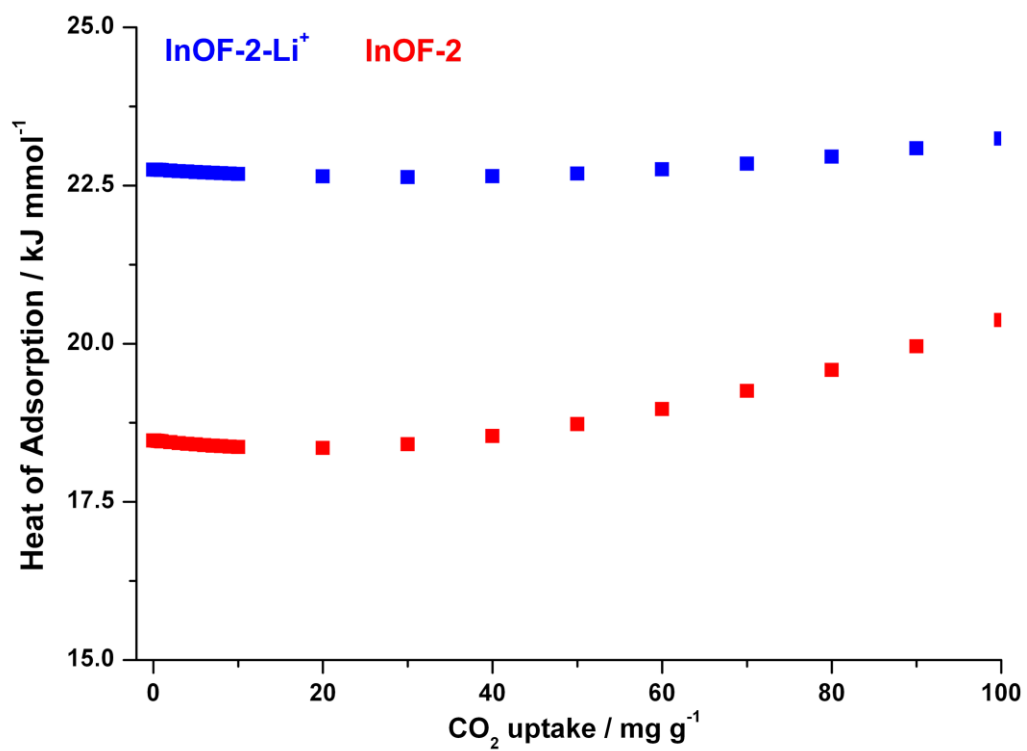
Figure S21. CO_2 heat of adsorption for **InOF-2-Li$^+$ (blue)** and **InOF-2 (red).**
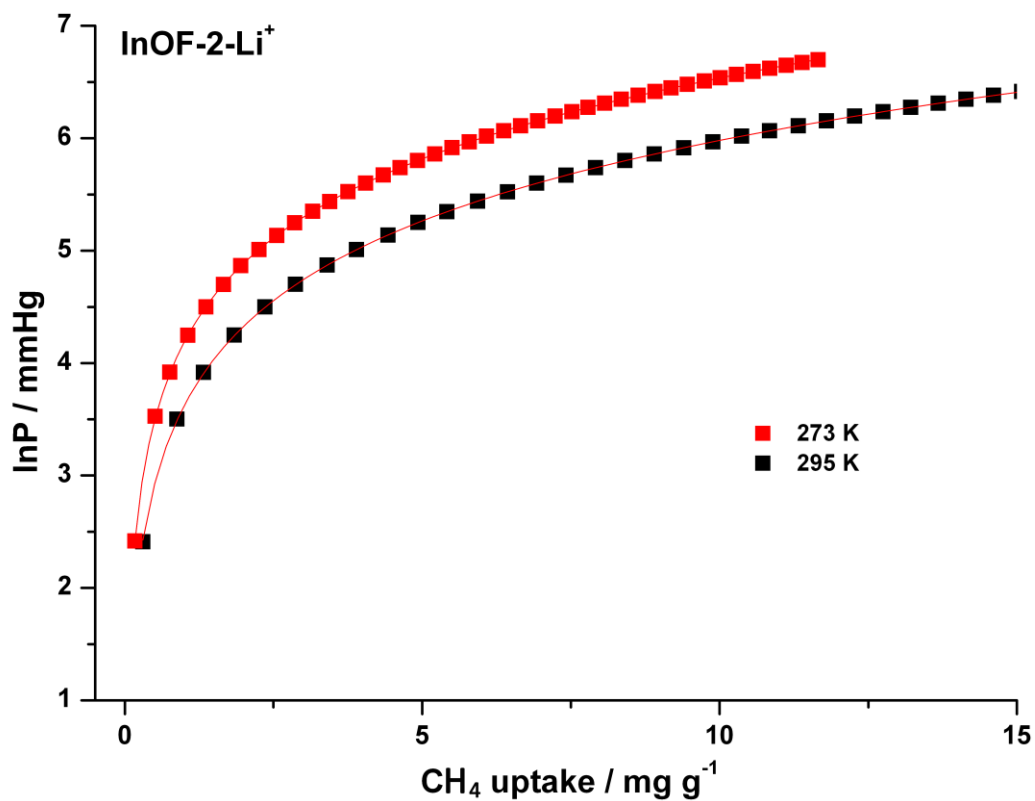
Calculation of heats of adsorption for CH_4

Figure S22. Nonlinear curve fitting of CH_4 adsorption isotherms for **InOF-2** at 273 K and 295 K.

$y=\ln(x)+1/k*(a0+a1*x+a2*x^2+a3*x^3+a4*x^4+a5*x^5)+(b0+b1*x+b2*x^2)$

		Value	Standard Error
	a0*	-1760.71152	11.3503
	a1*	27.22037	4.79923
	a2*	-0.39137	0.60865
	a3*	-0.37132	0.08528
	a4*	0.02798	0.00643
$\ln(P)$	a5*	-7.43025E-4	1.76062E-4
	b0*	10.2266	0.03934
	b1*	-0.09457	0.01641
	b2*	0.0088	0.00147
	k	273	0
	k	295	0

Figure S23. Nonlinear curve fitting of CH_4 adsorption isotherms for **InOF-2-Li$^+$** at 273 K and 295 K.

y=ln(x)+1/k*(a0+a1*x+a2*x^2+a3*x^3+a4*x^4+a5*x^5)+(b0+b1*x+b2*x^2)

		Value	Standard Error
	a0*	-2086.46801	9.35212
	a1*	21.94707	3.48978
	a2*	-1.84202	0.32171
	a3*	0.03371	0.02612
	a4*	-0.00139	0.0015
ln(P)	a5*	2.27766E-5	3.11054E-5
	b0*	11.25707	0.03261
	b1*	-0.06745	0.01207
	b2*	0.00528	9.42871E-4
	k	273	0
	k	295	0
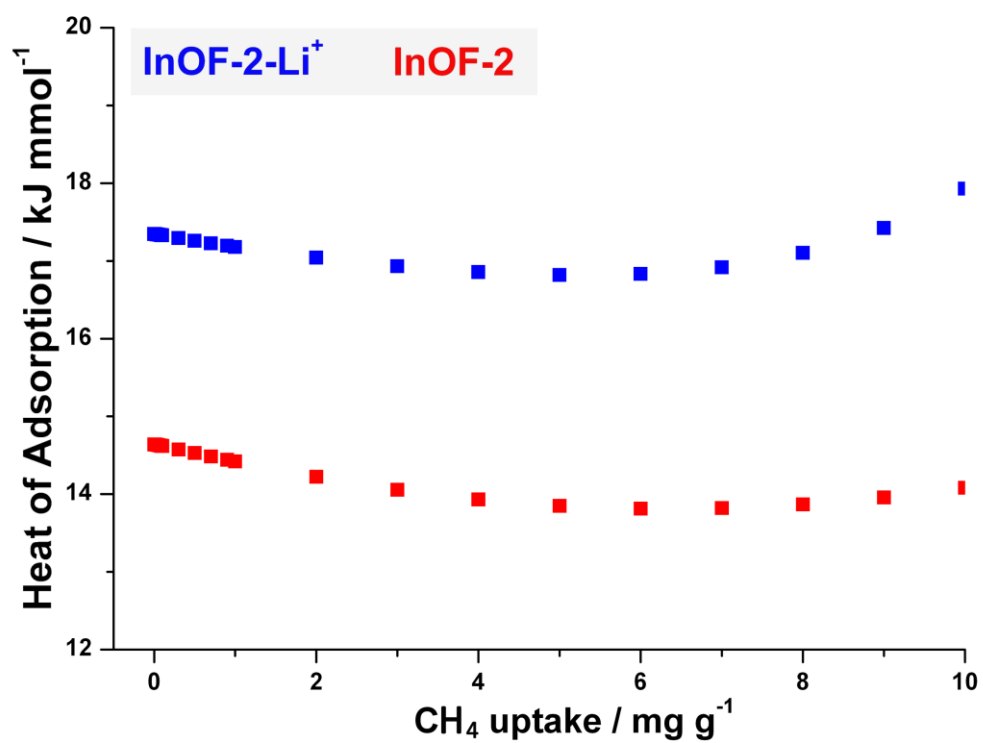
Figure S24. CH_4 heat of adsorption for **InOF-2-Li$^+$ (blue) and InOF-2 (red).**

S9. Single gas adsorption measurements

9.1. H$_2$ uptake measurements
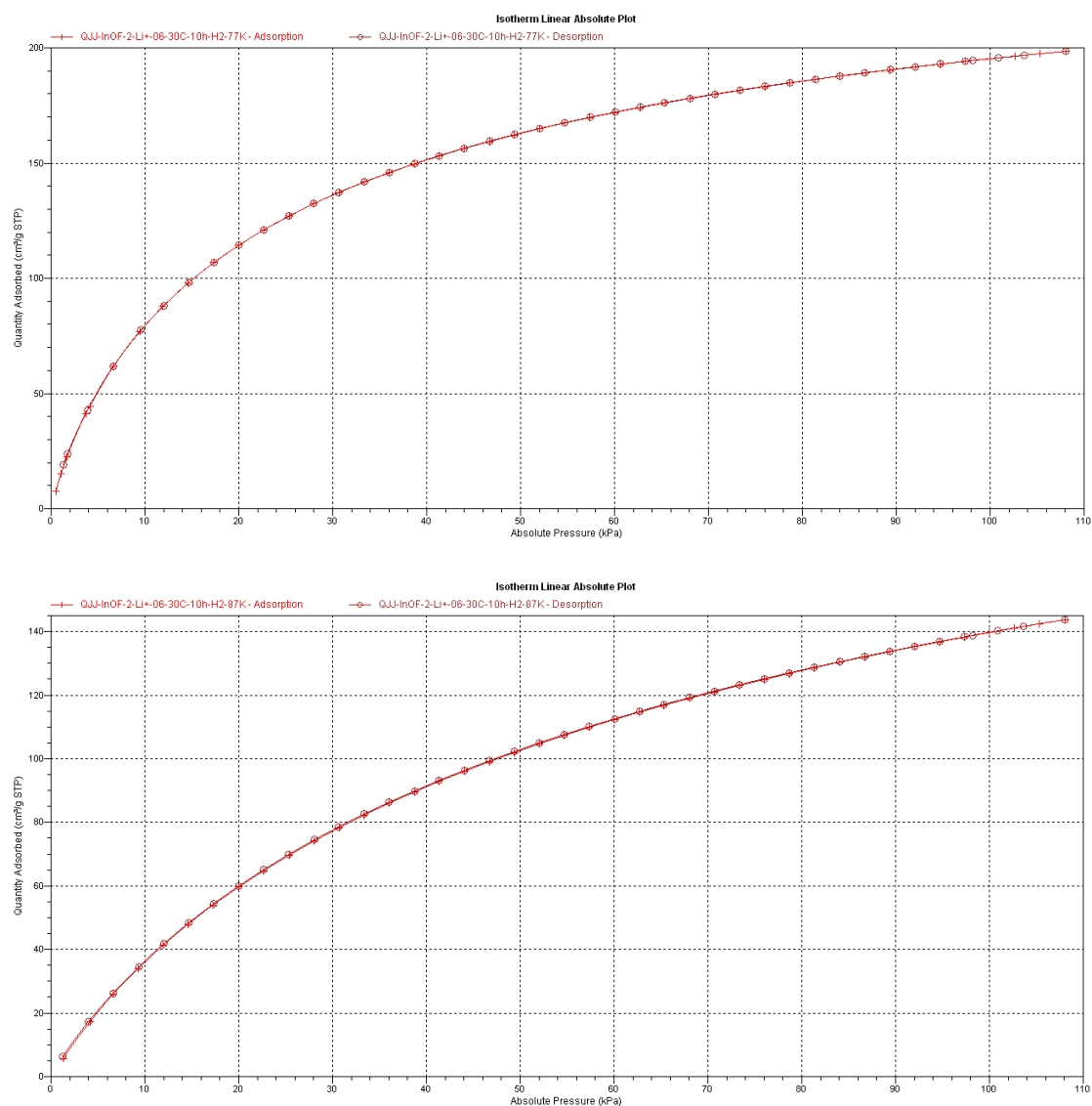
Figure S25. At 273/295 K, H$_2$ sorption of I **InOF-2-Li$^+$** activated at 303 K for

10h.

Isotherm Linear Absolute Plot

QJJ-InOF-2-Li+-06-50C-10h-H2-77K - Adsorption   QJJ-InOF-2-Li+-06-50C-10h-H2-77K - Desorption

Isotherm Linear Absolute Plot

QJJ-InOF-2-Li+-06-50C-10h-H2-87K - Adsorption   QJJ-InOF-2-Li+-06-50C-10h-H2-87K - Desorption
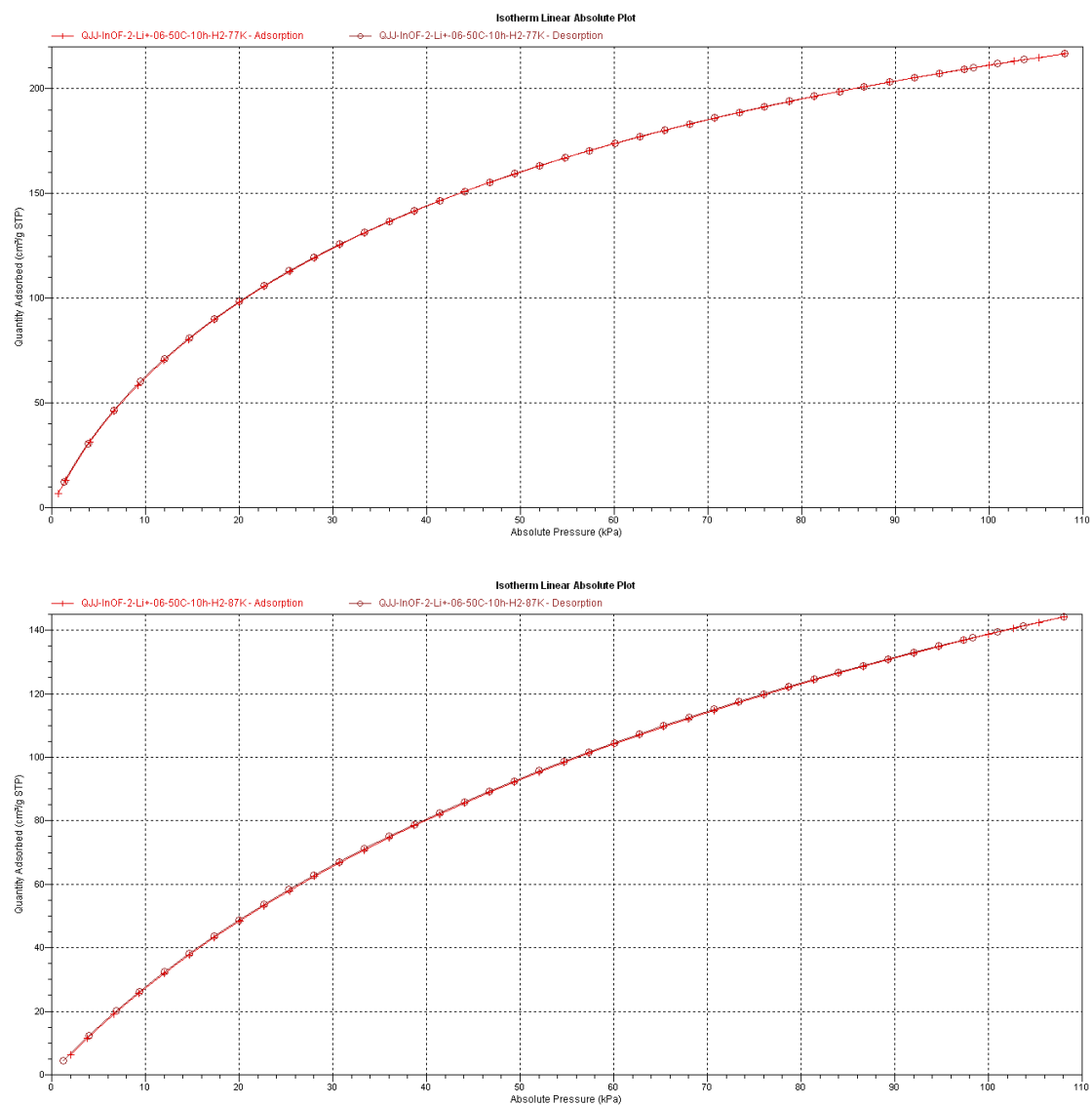
Figure S26. At 273/295 K, H_2 sorption of I **InOF-2-Li$^+$** activated at 323 K for

10h.
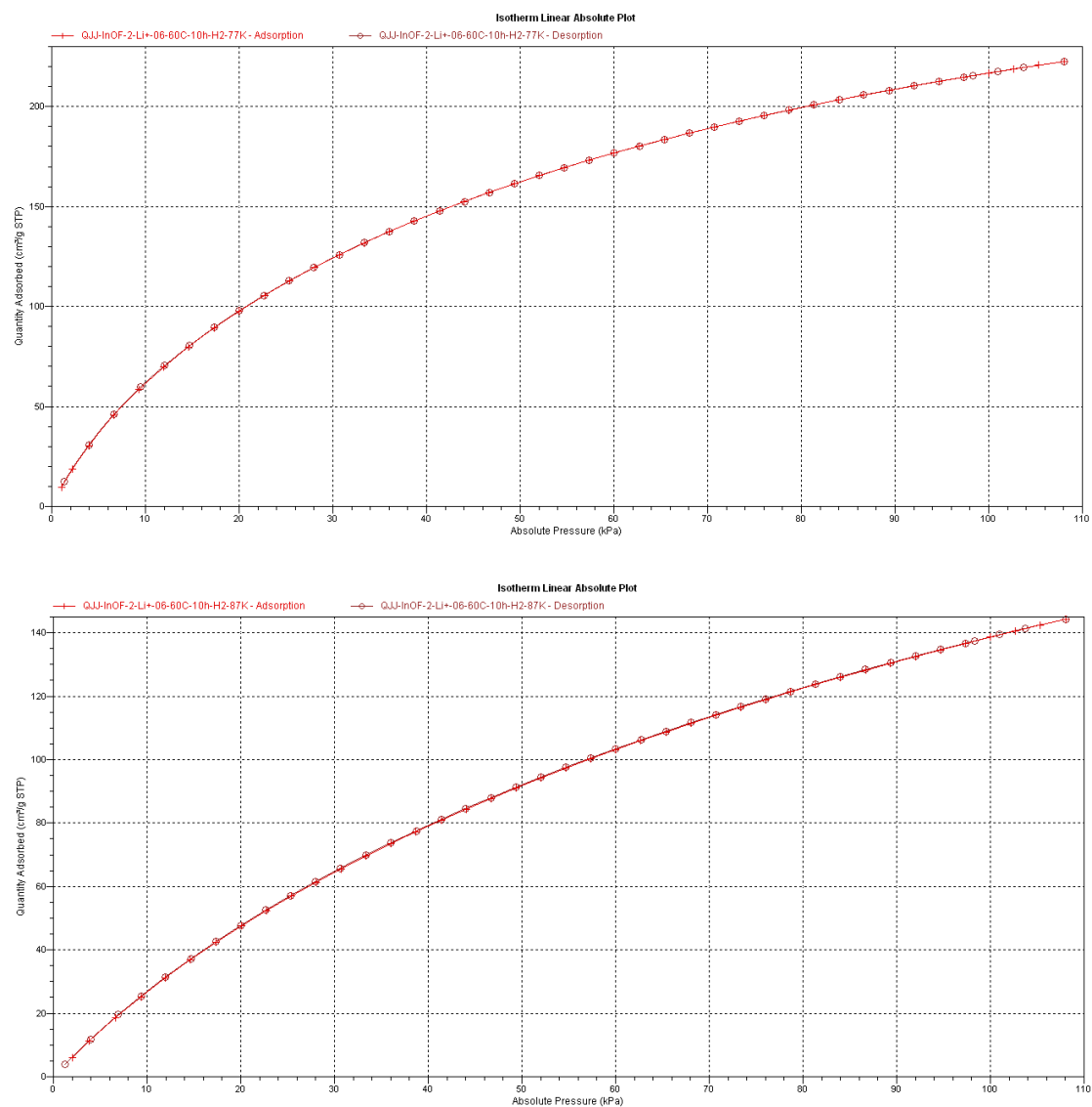
Figure S27. At 273/295 K, H$_2$ sorption of I **InOF-2-Li$^+$** activated at 333 K for 10h.
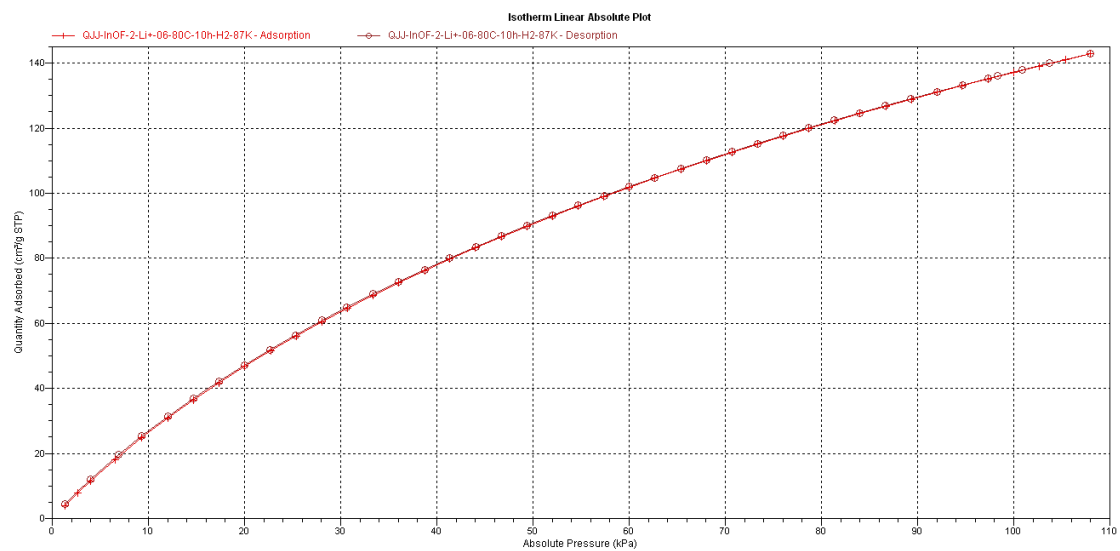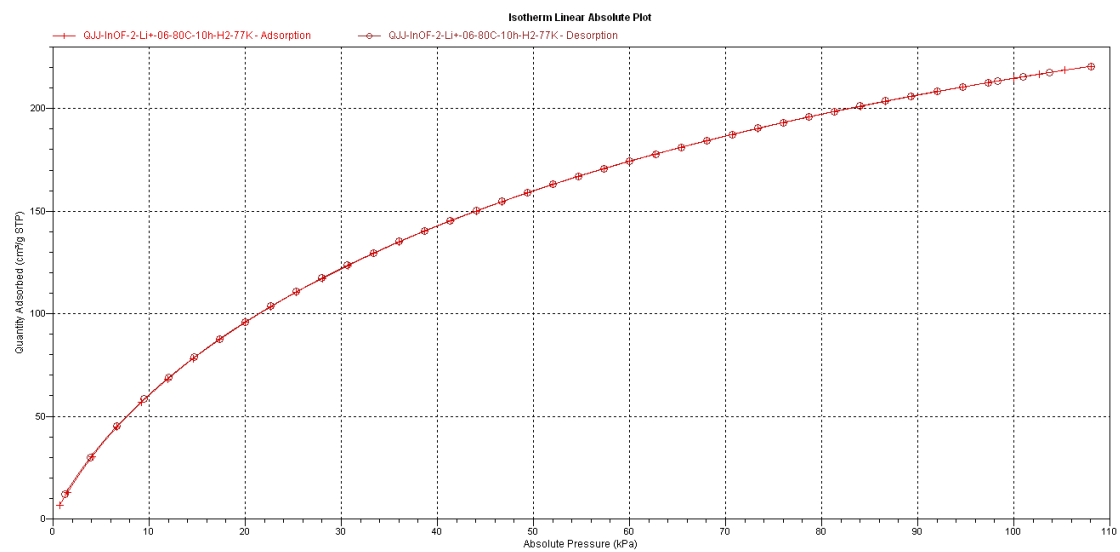
Figure S28. At 273/295 K, H_2 sorption of I **InOF-2-Li$^+$** activated at 353 K for 10h.
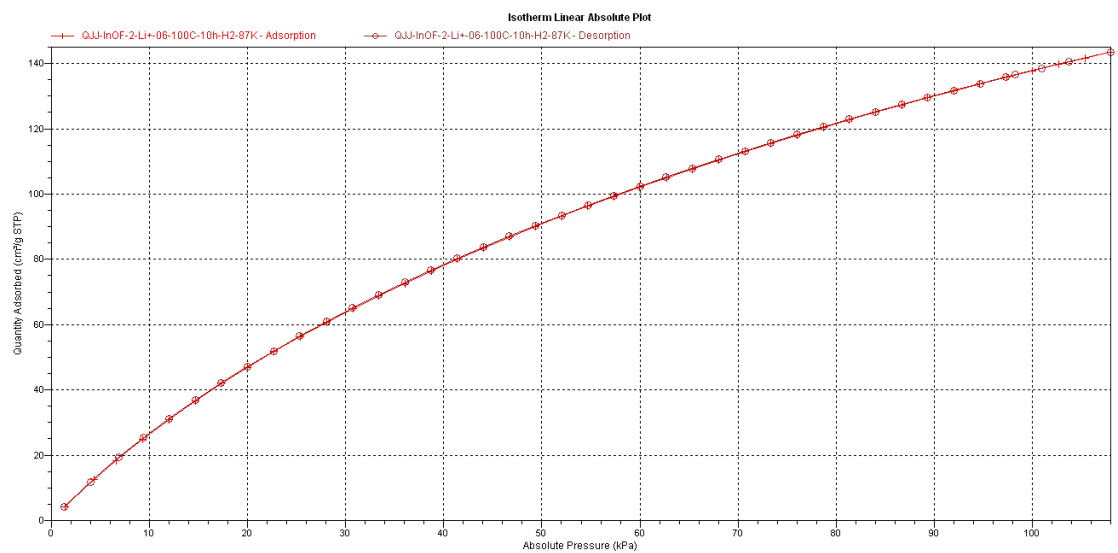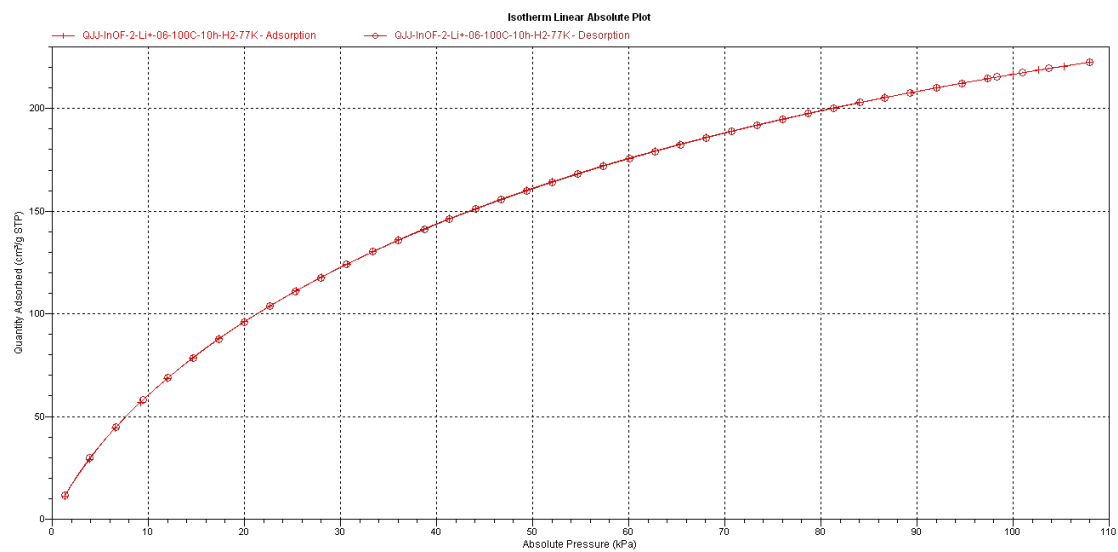
Figure S29. At 273/295 K, H_2 sorption of I **InOF-2-Li$^+$** activated at 373 K for 10h.

9.2. CO$_2$ uptake measurements
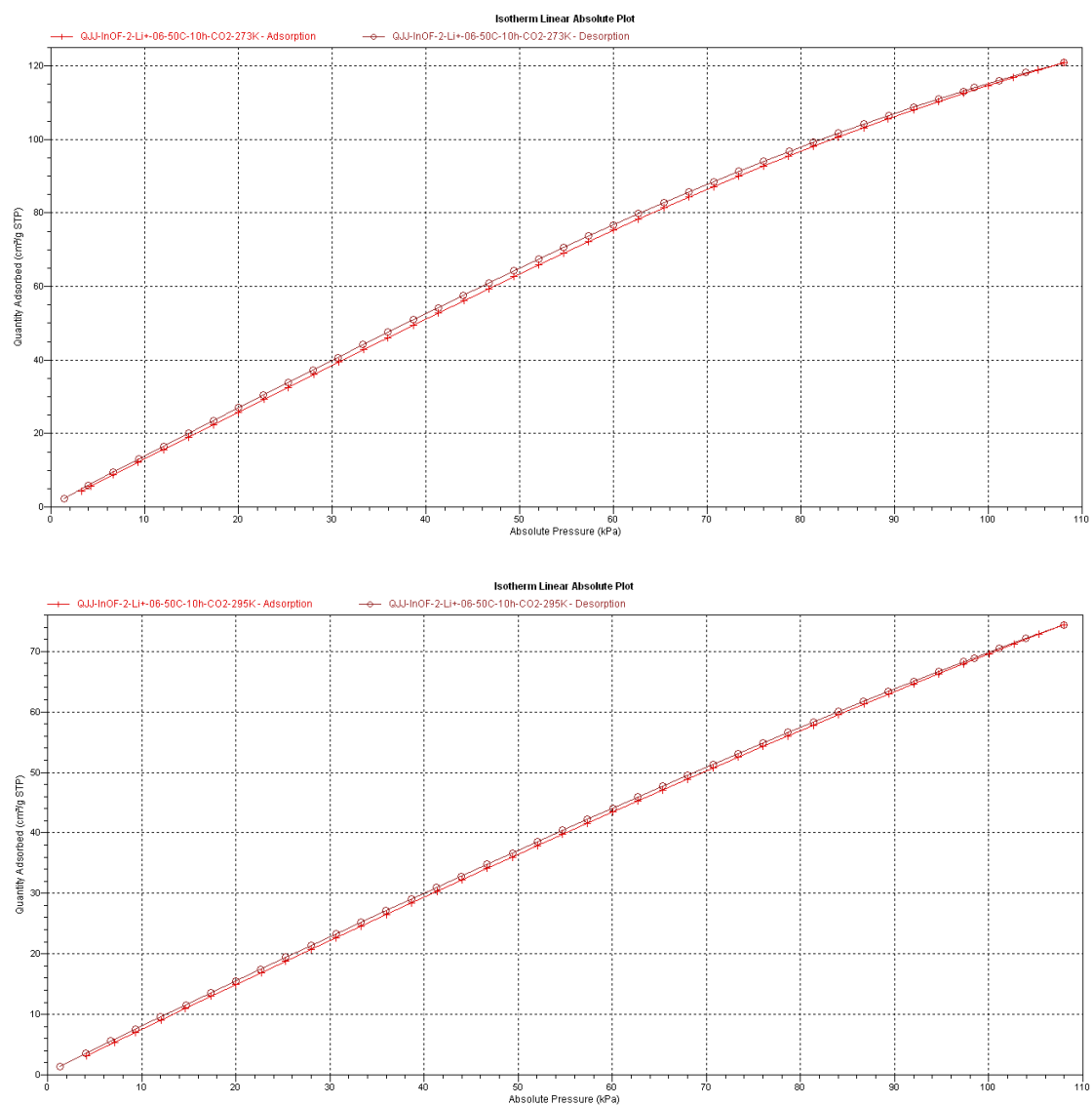
Figure S30. At 273/295 K, CO$_2$ sorption of I **InOF-2-Li$^+$** activated at 323 K for

10h.

S31
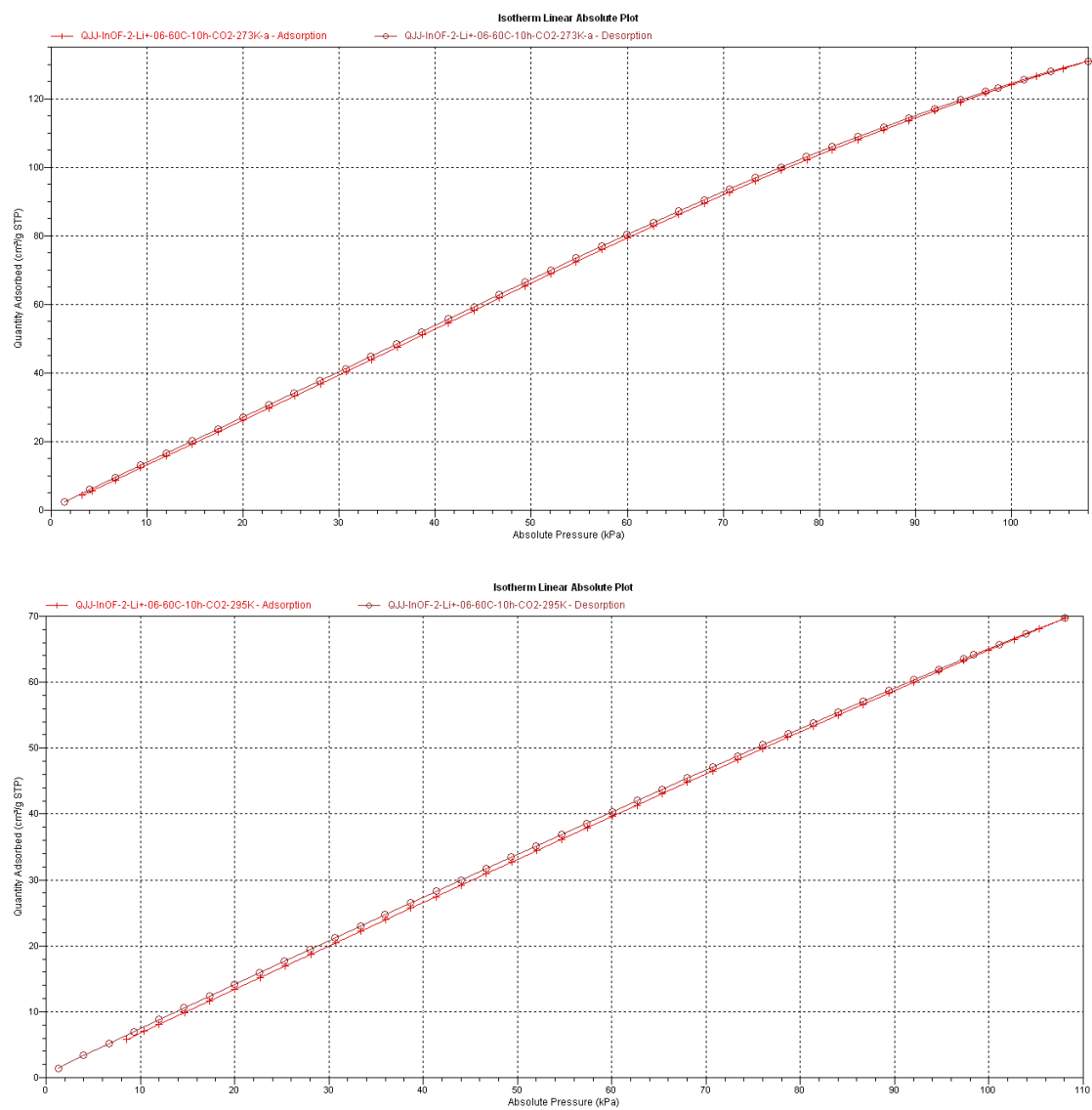
Figure S31. At 273/295 K, CO_2 sorption of I **InOF-2-Li$^+$** activated at 333 K for 10h.

S32
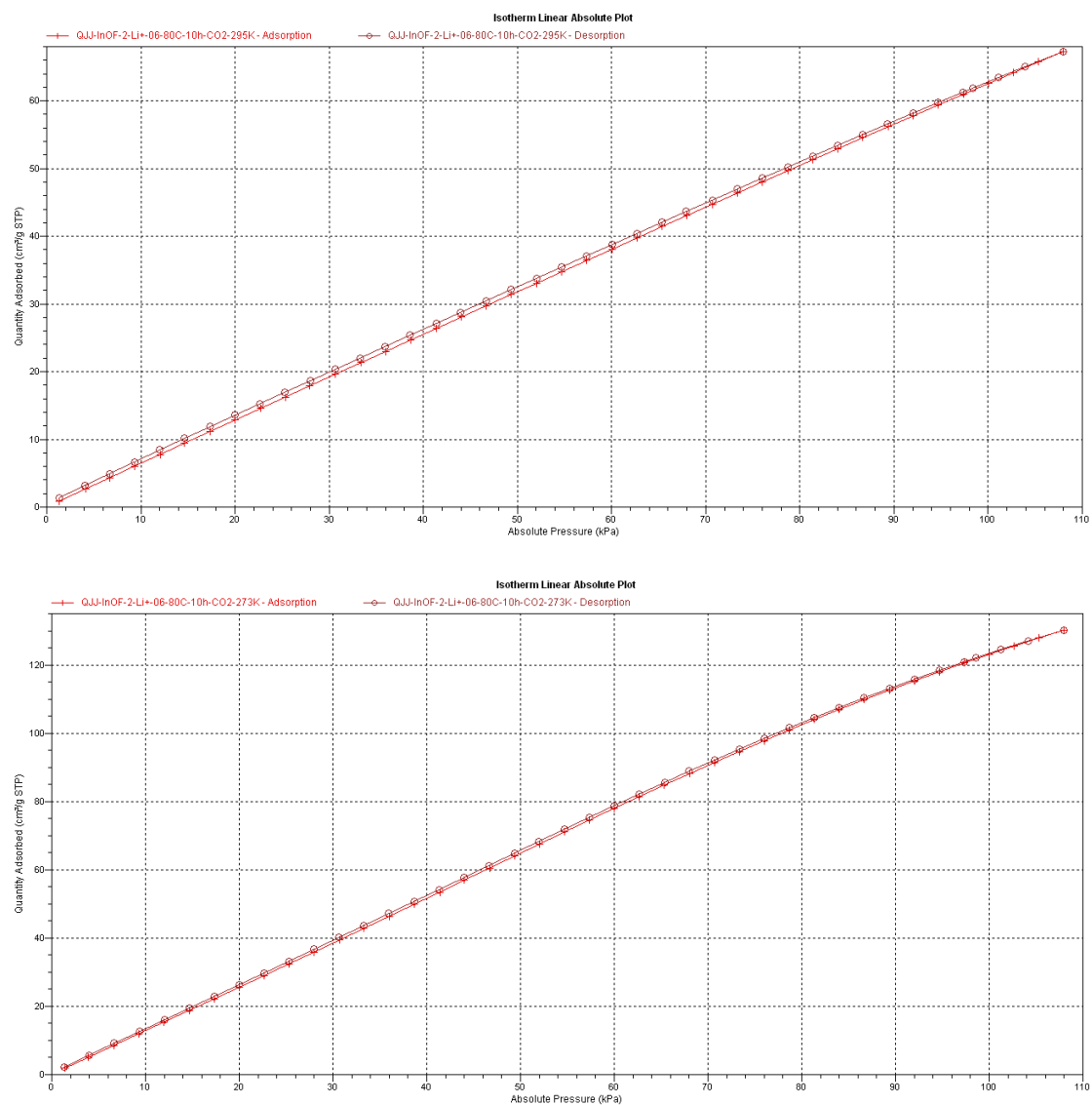
Figure S32. At 273/295 K, CO_2 sorption of I **InOF-2-Li$^+$** activated at 353 K for 10h.
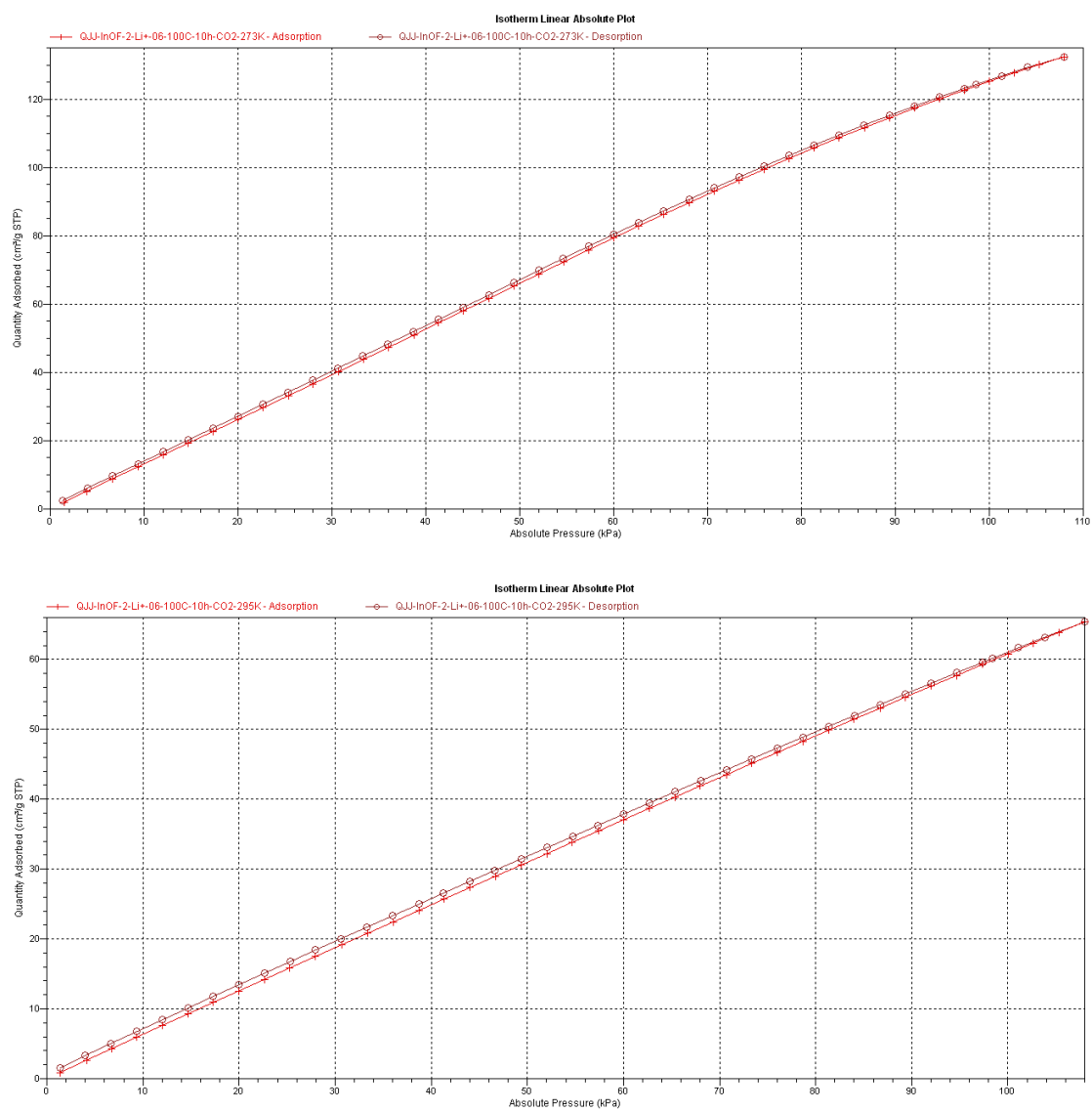
Figure S33. At 273/295 K, CO_2 sorption of I **InOF-2-Li$^+$** activated at 373 K for 10h.

9.3. CH$_4$ uptake measurements
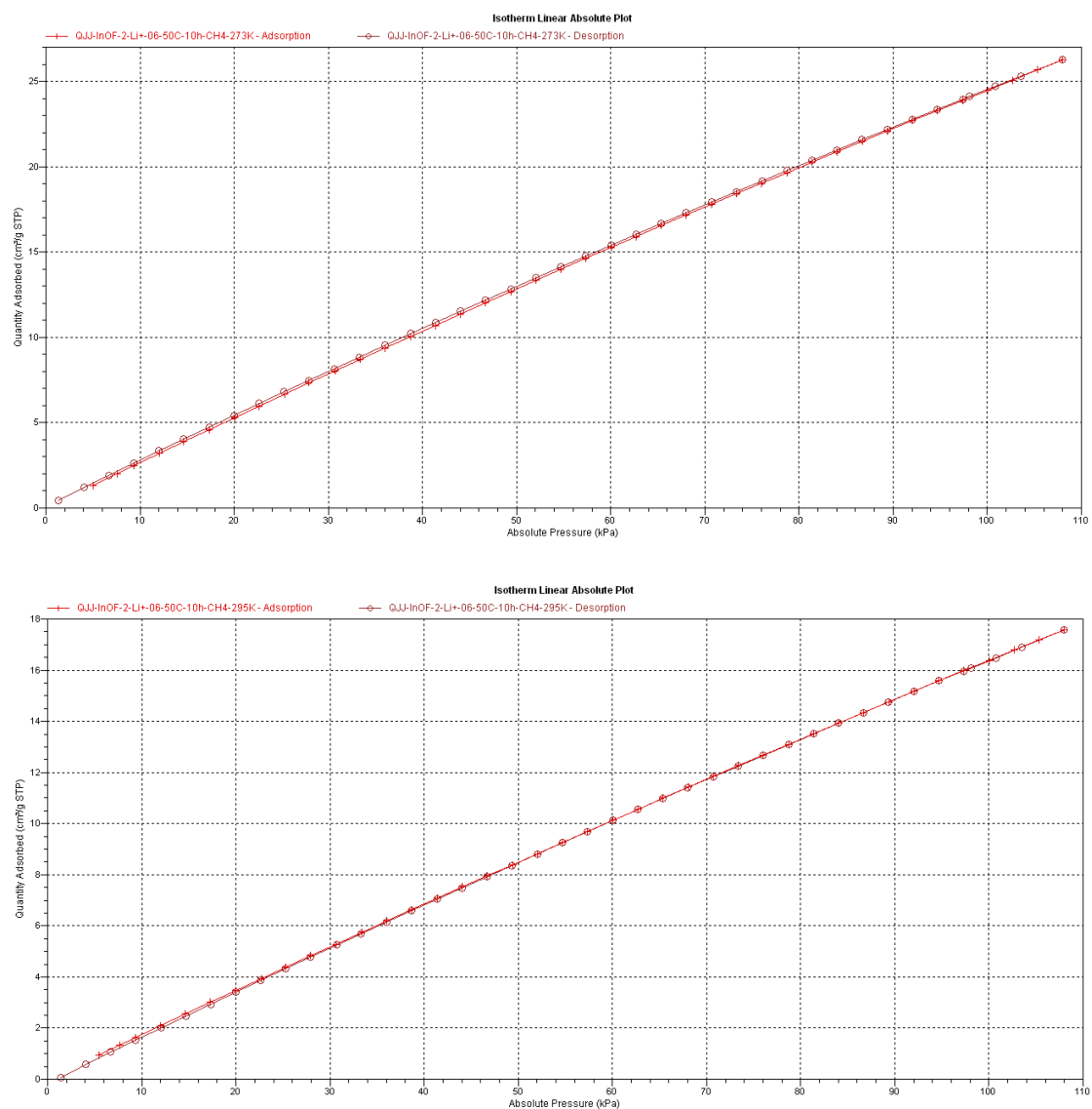
Figure S34. At 273/295 K, CH$_4$ sorption of I **InOF-2-Li$^+$** activated at 323 K for 10h.
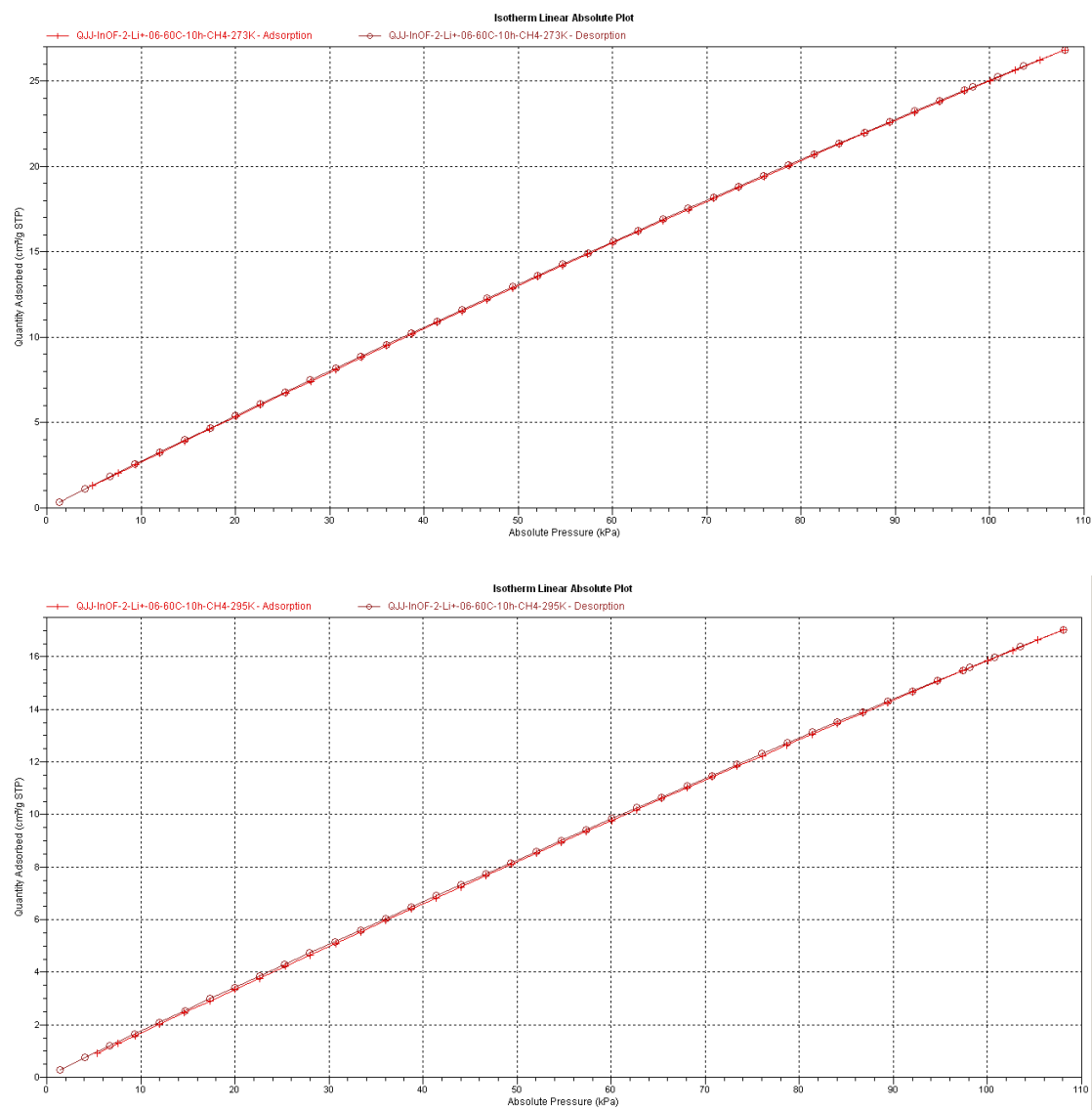
Figure S35. At 273/295 K, CH_4 sorption of I **InOF-2-Li$^+$** activated at 333 K for 10h.
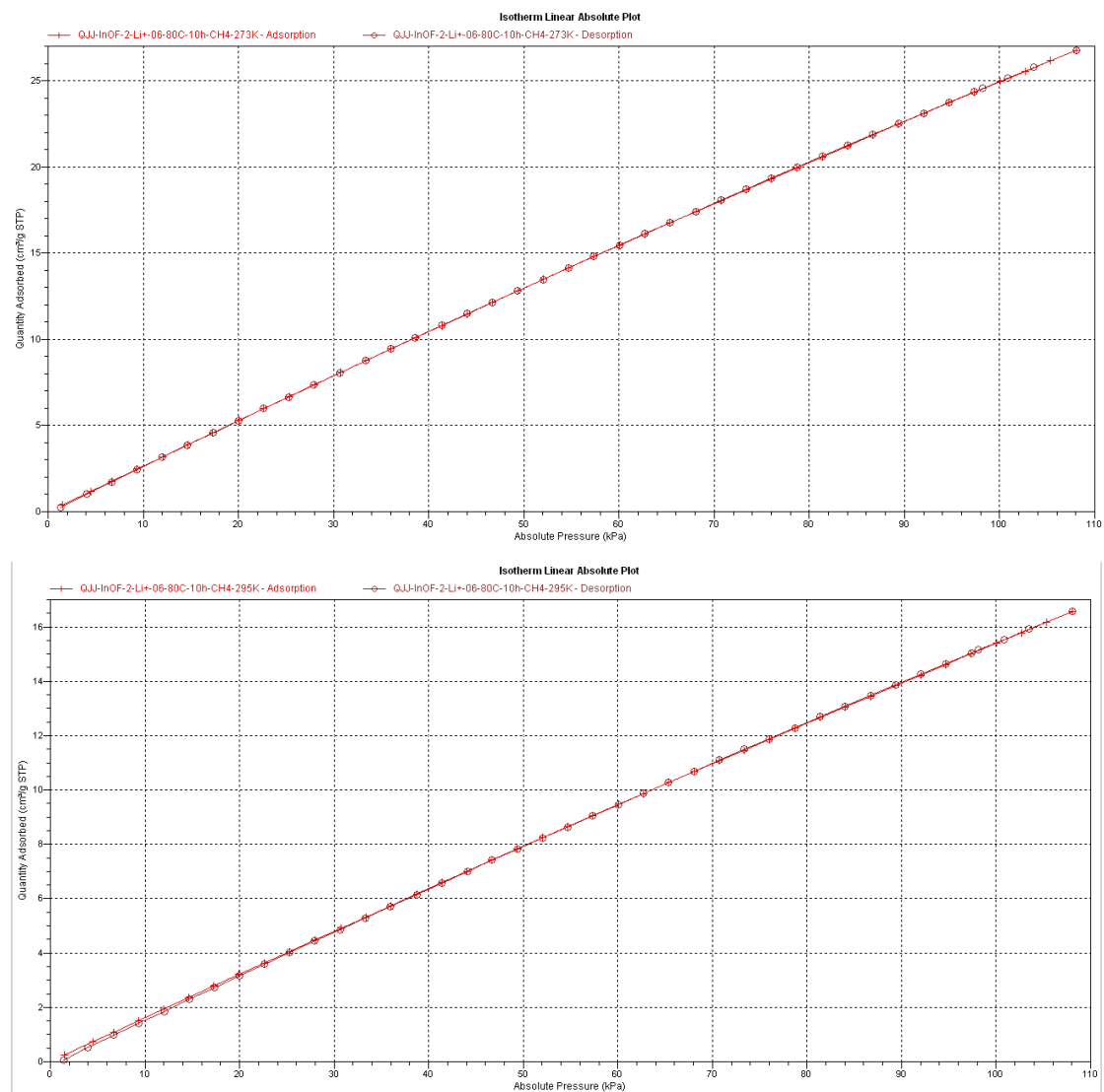
Figure S36. At 273/295 K, CH_4 sorption of I **InOF-2-Li$^+$** activated at 353 K for 10h.
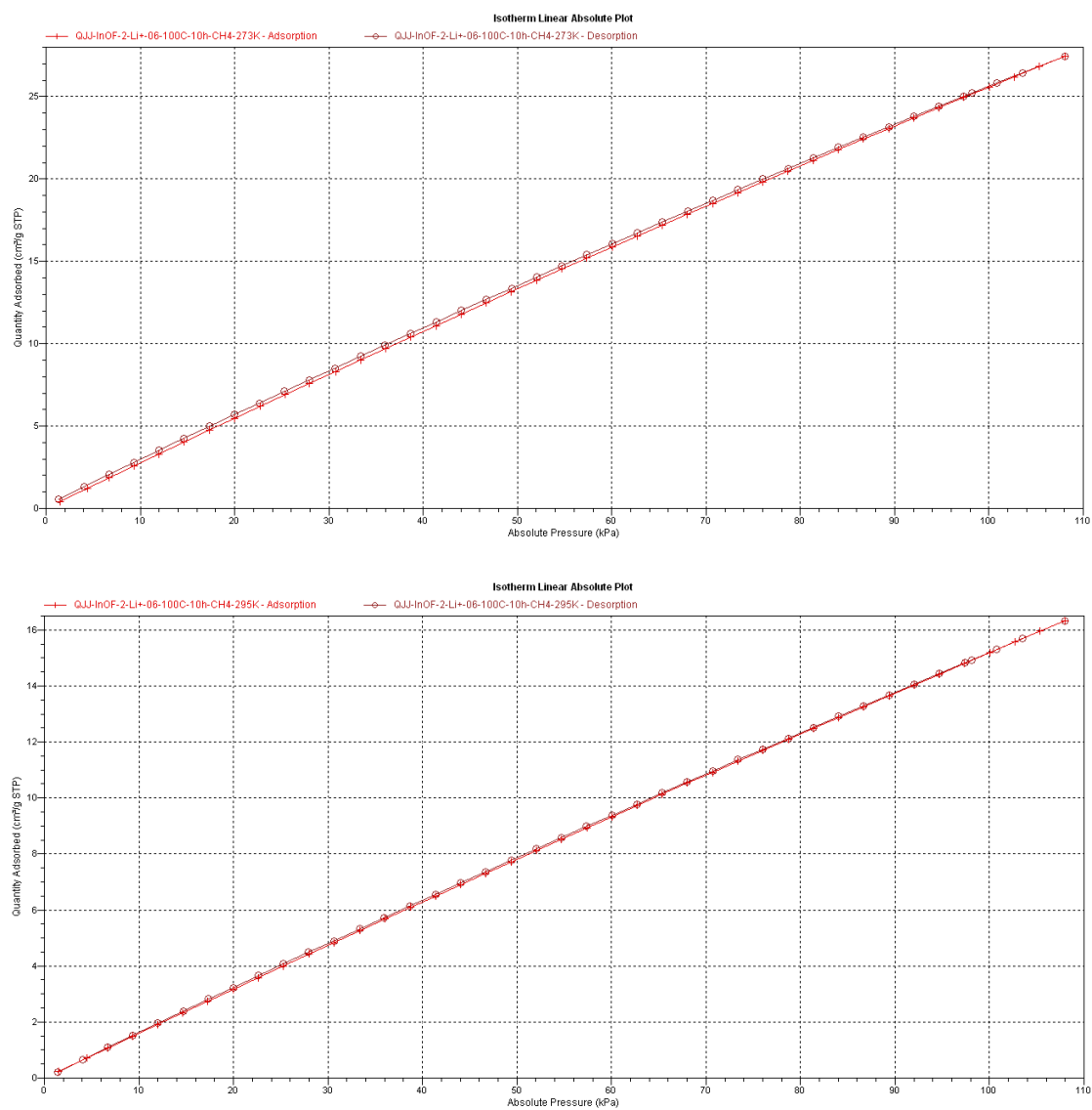
Figure S37. At 273/295 K, CH$_4$ sorption of I **InOF-2-Li$^+$** activated at 373 K for 10h.

9.4. N_2 uptake measurements
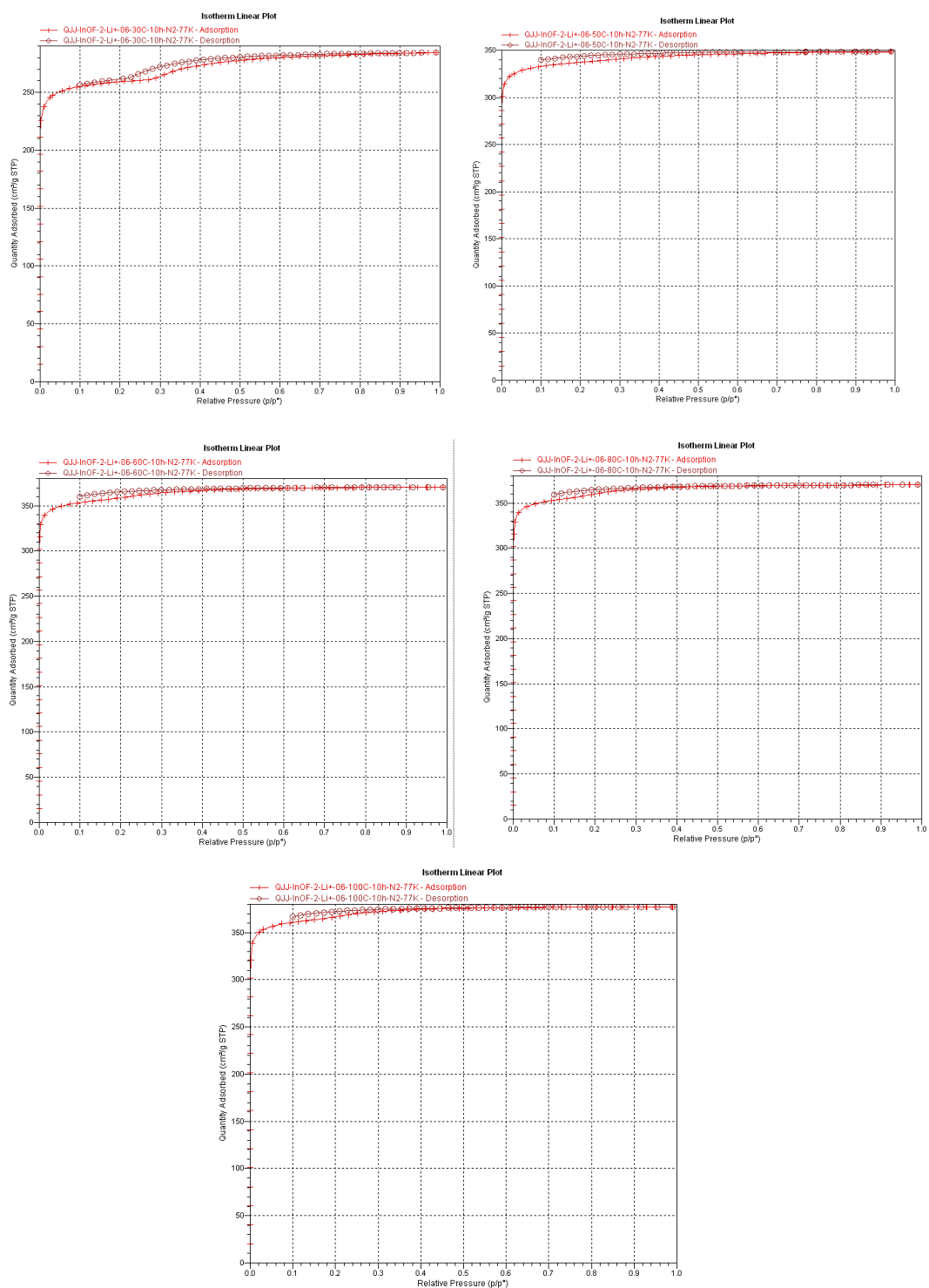

Figure S38. At 77 K, N_2 sorption of I **InOF-2-Li$^+$** activated at from 303 to 373 K

for 10h.

S10. References.

[S1].Yang, S.; Lin, X.; Blake, A. J.; Thomas, K. M.; Hubberstey, P.; Champness, N. R.; Schroder, M., *Chem. Commun.* **2008**, 6108.

[S2].Qian, J. J.; Jiang, F. L.; Yuan, D. Q.; Wu, M. Y.; Zhang, S. Q.; Zhang, L. J.; Hong, M. C., *Chem. Commun.* 2012, **48**, 9696-9698.

[S3] Sheldrick, G. M. SHELXS-97, Programs for X-ray Crystal Structure Solution; University of Göttingen: Germany, **1997**.

[S4] (a) A. L. Spek, *J. Appl. Crystallogr.* **2003**, *36*, 7; (b) P. v.d. Sluis and A. L. Spek, *Acta Crystallogr., Sect. A*, **1990**, *46*, 194.

[S5] ASAP 2020 Accelerated Surface Area and Porosimetry System Operator's Manual V4.00, Appendix C, C-43.